CHALMERS
UNIVERSITY OF TECHNOLOGY

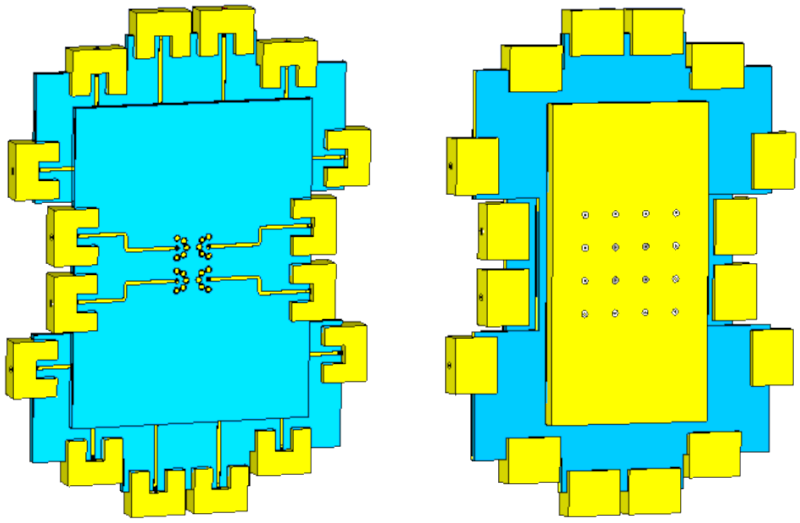

Integration of 4x4 circularly-polarized array to Tx/Rx circuitry with MetaCoax Technology

Master's thesis in Wireless, Photonics and Space Engineering

Xadia Catalina Perez Anguiano

DEPARTMENT OF ELECTRICAL ENGINEERING,

ANTENNA RESEARCH GROUP

CHALMERS UNIVERSITY OF TECHNOLOGY
Gothenburg, Sweden 2021
www.chalmers.se

Master's thesis in Wireless, Photonics and Space Engineering

2021

Integration of 4x4 circularly-polarized array to Tx/Rx circuitry with MetaCoax Technology

Xadia Catalina Perez Anguiano

CHALMERS
UNIVERSITY OF TECHNOLOGY

Department of Electrical Engineering
Antenna Research Groups
CHALMERS UNIVERSITY OF TECHNOLOGY
Gothenburg, Sweden 2021
www.chalmers.se

Integration of 4x4 circularly-polarized array to Tx/Rx circuitry with MetaCoax Technology

Xadia Catalina Perez Anguiano

Supervisors: Prabhat Khanal (Chalmers University of Technology)
Sadegh Mansouri (Gapwaves)
Jian Yang (Chalmers University of Technology)

Examiner: Jian Yang (Chalmers University of Technology)

Master's thesis in Wireless, Photonics and Space Engineering, 2021
Department of Electrical Engineering
Antenna Research Group
CHALMERS UNIVERSITY OF TECHNOLOGY
Gothenburg, Sweden 2021
www.chalmers.se

Acknowledgements

I would like to thank my supervisors Prabhat Khanal, Sadegh Mansouri and my examiner Jian Yang for providing me with invaluable guidance and support during this thesis project. I appreciate all the meetings to discuss the work and its direction. Also, I want to thank Gapwaves for giving me the opportunity to participate in a project with them.

Finally, I want to thank my family and friends who kept me motivated throughout the thesis. The last two years have been life changing, I could not have done it without their unconditional love and support.

Xadia Catalina Pérez Anguiano, Gothenburg, October 2021

Integration of 4x4 circularly-polarized array to Tx/Rx circuitry with MetaCoax Technology

Xadia Catalina Perez Anguiano

Abstract

In the field of communication technology, there is a rising demand of a variety of applications and services that requires transmission and reception of high amounts of data at high data rates with support for several users. A critical enabling technology to achieve those requirements in current wireless systems is the Ultra-Wideband (UWB) millimeter wave (mmWave) antenna system technology.

One particular characteristic of the large UWB mmWave antenna arrays is the very limited element spacing, causing that the Tx/Rx modules cannot be easily fitted into those small spaces. Also, such antennas are intended to be integrated with Tx/Rx modules at low production costs which, as overall, is a challenging task.

There are some solutions to the space limitation of the UWB antenna array integration, but they have some drawbacks like appearance of grating lobes, non-linear effects, bulky fiber connections, heat dissipation problems, etc. Thus, a new integration technology is highly demanded to overcome such difficulties and limitations.

In this thesis project, a new integration technology called MetaCoax is studied and tested. MetaCoax makes use of capacitive coupling by creating a gap between conductive elements and a metasurface in order to stop leakage and mutual coupling.

Preliminary tests show that the MetaCoax integration has low losses, compact geometry, it is flexible regarding size and configuration, it is cost effective, the air gaps between PCB layers could reduce heat dissipation issues and it can successfully address the space limitation problem due to the small separation between antenna array elements.

Keywords: Integration technology, UWB, mmWave antenna arrays, MetaCoax.

Contents

List of Figures

List of Tables

1

1. Introduction

This master thesis is oriented to study and design an integration board for an existing circularly polarized phased array based on PCB, applying a technology called MetaCoax, which is a contactless capacitively-coupled gapwave coaxial coupling.

In Chapter 2, the state-of-the-art of integration technologies is discussed. Some benefits and also drawbacks of different integration technologies are mentioned, as well as the importance of having a new integration option for antenna arrays.

Chapter 3 covers the concept of the MetaCoax technology, a novel approach to integrate antenna arrays and Tx/Rx modules. The selected methodology of this thesis project was aimed to test and evaluate an antenna array integration board based on MetaCoax and it is also included in Chapter 3.

Two models were simulated and they were tested under several conditions of interest, such as PCB misalignment and bonding layer incorporation. The procedure and results of such tests are described in the methodology section.

Chapter 4 includes a detailed discussion of the simulation results, procedures, project findings, main faced challenges and future work.

Chapter 5 summarize the final conclusions of the project, it includes general thoughts about MetaCoax implementation in integration networks, its advantages, downsides and key findings.

2

2. State-of-the-Art of Integration technologies

In the field of communication technology, there is a rising demand of a variety of applications and services that require transmission and reception of high amounts of data at high data rates with support for several users.

One of the critical enabling technologies for achieving high data rates in current wireless systems is the Ultra-Wideband (UWB) millimeter wave (mmWave) antenna system technology. UWB is a wireless technology used for transferring high bandwidth data at high rates over short ranges (Rahayu, Rahman, Ngah, & Hall, 2008). And the mmWave bands, typically defined within the frequency range of 30–300 GHz, are particularly useful in order to achieve the high bandwidth requirement of new and emerging applications.

The antenna technology used in UWB at mmWave bands have high gains and capability of having multiple independently steerable beams intended for multi user services. One particular characteristic of the large UWB mmWave antenna arrays is the very limited element spacing, causing that the Tx/Rx modules cannot be easily fitted into those small spaces. Also, such antennas are intended to be integrated with Tx/Rx modules at low production costs which, as overall, is a challenging task.

There are some solutions to the space problem of the UWB antenna array integration and they are divided into three categories: tiling technology, RF-optic transformers or Vertical Cavity Surface Emitting Laser (VCSEL) technology and direct multilayer PCB technology.

The tiling technology consists in the combination of several elements into a sub-array for one Tx/Rx module. In this way, by creating several sub-arrays, it is possible to create an integration network for the whole antenna array even if the space between elements is limited.

However, the maximum beam scan angle and the bandwidth become reduced due to the appearance of grating lobes with a large sub-array spacing. Those grating lobe effects may appear because of interruption of the overall periodic structure due to the physical connection between mechanical subarrays of finite size (Bhowmik & Fulton, 2016).

The RF-optic transformers technology employs VCSEL to transfer RF signal to optic signal, combining 4 array element RF channels into one optical fiber. This technology can fit into the small space between antenna elements and it can easily achieve heat dissipation requirements (Zhongxia & et. al., 2017).

However, this method has also some constrains. The optoelectronics-antenna integration based on VCSEL has been demonstrated below 6 Ghz (Cryan & et. al., 2004), but there is no much work at frequencies higher than the 3 dB cutoff frequency. This cutoff frequency has been estimated to be at 28 GHz according to some studies (Safaisini & et. al., 2012) (Westbergh & et. al., 2012). Also, this integration technology has been used only for signal reception (Zhongxia & et. al., 2017), presents non-linear effects (Nazhan & et. al., 2021) and employs bulky fiber connections.

The direct multilayer PCB technology uses vias as the coupling transmission lines to connect array elements to Tx/Rx modules on different PCB layers (Jaehyun Choi, 2020). The use of thin substrates causes degradation in the gain of the antenna and a multilayer structure can be used to reduce it (Eu & et. al., 2017). Another benefit of the multilayer PCB technology is its size. Although a multilayer PCB is thicker, it allows to have generally smaller dimensions than a single PCB.

Nevertheless, the multilayer technology has the following drawbacks: a big transmission loss (>10 dB) through vias (Fukumori & et. al., 2012), it is difficult to fabricate a PCB with several layers for mmWave frequencies due to the small dimensions of the different components and it has severe heat dissipation problems due to the solid multilayer structure.

After revising the tiling technology, the RF-optic transformers or VCSEL technology and the direct multilayer PCB technology, it is clear that a new integration technology is highly demanded to overcome all the difficulties and limitations of the different approaches mentioned above.

Therefore, in this thesis project a new integration technology called MetaCoax is explored and tested. This technology is a promising technique with some interesting features that can effectively contribute to the state-of-the-art of the integration technologies.

3

3. MetaCoax Technology

MetaCoax is a technology that has two main variants: the partially contact MetaCoax and the fully contactless MetaCoax. The structure of the two MetaCoax variants are shown in Figure 1.

The partially contact MetaCoax combines three technologies: air coaxial transmission lines, flip chip ball soldering joints and metasurfaces. This approach allows to achieve a low-loss and low-cost signal connection between the PCB patch and the air coaxial transmission line.

The inner conductor of the air coaxial transmission line is connected to the patch by a flip chip soldering joint and the outer conductor is contactless to the PCB with a small air gap. The leakage and mutual coupling between the different air coaxial transmission lines is reduced by employing a metasurface on the MetaCoax array.

The fully contactless MetaCoax makes use of capacitive coupling by creating a gap between the inner conductor and the patch. It also uses a metasurface on the surface of the MetaCoax array to stop leakage.

Some benefits of both variants of the MetaCoax technology after some preliminary tests are: it has low loss, it has a compact geometry, it is flexible regarding size and configuration, it is cost effective, the air gaps between PCB layers reduce heat dissipation issues and it can successfully address the space limitation problem due to the small separation between the different antenna array elements.

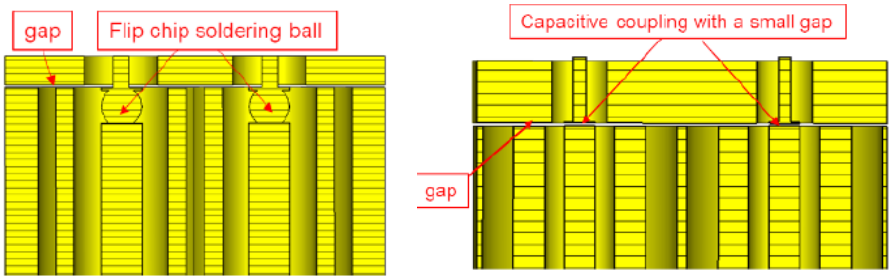

Figure 1. Partially contact MetaCoax (left) and Fully contactless MetaCoax (right).

The fully contactless MetaCoax technology is applied in this thesis project, it was used in the integration network design of an antenna array. It is expected to have a good performance while keeping all the advantages found during the preliminary tests of the novel integration technology.

The method used in this project covers the design and simulation of the integration board for an existing 4x4 antenna array using CST software, an electromagnetic design tool. The aimed frequency range for the model is 17-22 GHz, which is within the denominated K band. K band is considered as a microwave band, but is not uncommon to find references that mentions K band alongside the mmWave bands in their studies (GSMA, 2021).

Since a whole 4x4 integration network requires to connect 16 ports and generate a model with several layers, the design procedure and simulations were divided in stages to organize all the work.

The first stage covers the design of a 2x2 integration network. The 2x2 model is less complex and requires less simulation processing time than a 4x4 model. Therefore, the 2x2 model can be easily manipulated by changing and optimizing its parameters. In this way, the performance of the model is also easier to analyze.

The second stage was focused on extending the 2x2 model to a 4x4 model. The design of the 4x4 model involved more layers and the adjustment of the microstrip lines in order to have 4 port connectors per each side of the integration board while keeping a mirror type geometry. In the next sections, the design and structure details of both models are described.

The fully contactless MetaCoax technology was applied in the design of the integration network, thus there are air gaps in between sections of the model. In a physical prototype, air gaps can be implemented by using screws to attach each PCB section leaving spaces between them. Nevertheless, it is also possible to use a bonding layer material to attach the different sections of the model. The usage of bonding layer materials to attach each section of the integration network was also studied during this thesis and its effects are described at the end of this chapter.

3.1 Design and model of 2x2 array integration with MetaCoax

The first step of the design stage was the creation of a 2x2 integration network model. The 2x2 model consisted of several layers as showed in Figure 2. This model can be divided into 2 general parts: the antenna interface and the integration or feeding network. The antenna interface has a metal layer and a PCB layer, coaxial connectors and via holes. The antenna interface was created for testing purposes during the design stage, but it has to be replaced with the actual model of an antenna array.

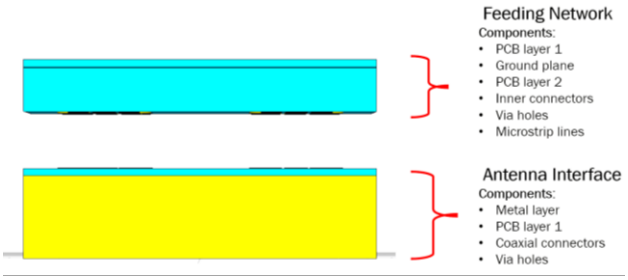

Figure 2. 2x2 model structure.

The feeding network has two PCB layers, a ground plane, inner connectors, via holes and microstrip lines. The feeding network and the antenna interface are separated by an air gap.

The material of the PCB layers is Rogers RT5880. The metal and ground planes, vias, pads, connectors and microstrip lines were modeled with copper. The dielectric material used in the antenna interface for the coaxial connector is PTFE.

Figure 3 a) shows the front and back view of the feeding network, where the red rectangles are the ports used for simulation. Figure 3 b) shows the front and back view of the antenna interface and Figure 3 c) shows a frontal view of both structures, the feeding network and the antenna interface together.

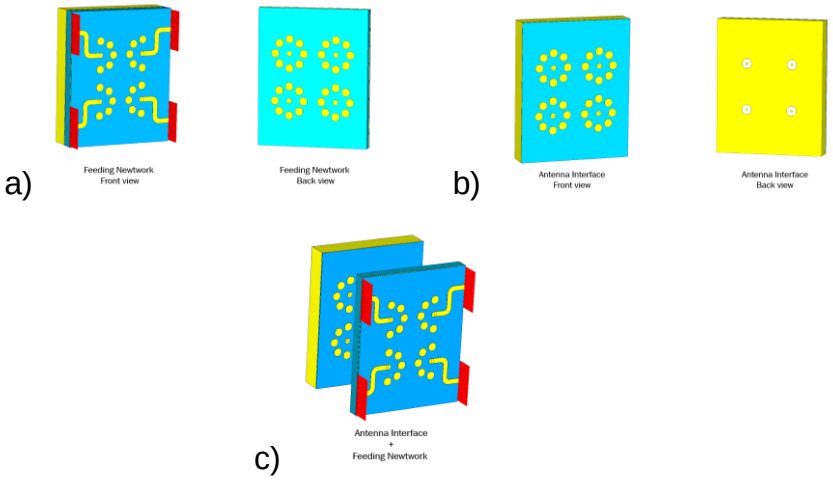

Figure 3. a) Feeding network views, b) Antenna interface views and c) Antenna and Feeding network view.

Figure 4. shows the cutting plane view of the model, which allows to visualize the inner parts of the structure. In this picture is possible to appreciate some of the via holes and coaxial connectors. The via holes around each coaxial connector were designed to stop leakage and mutual coupling. Each element is a mushroom-like electromagnetic band-gap structure, like the ones in (Zhang & et. al., 2020), whose dimensions are adjusted to obtain a good performance of the model within the frequency range 17-22 GHz.

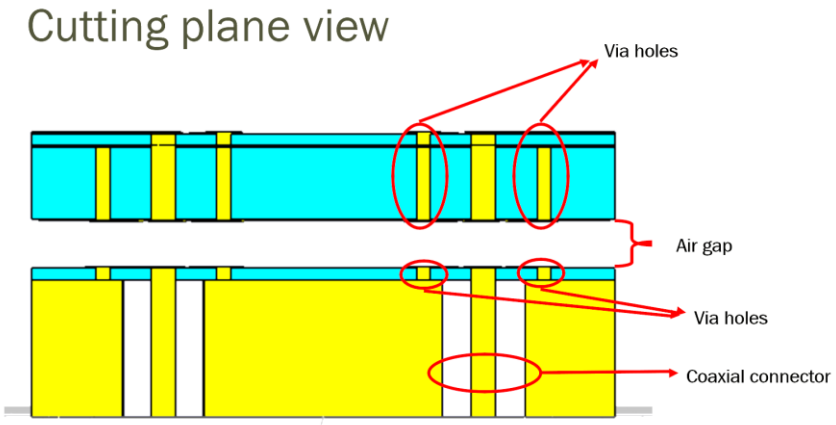

Figure 4. Cutting plane view of the 2x2 model.

Figure 5 is a close up of the area of a connector that communicates the antenna interface and the feeding network. The air gap size is considered as the space between the copper pads.

Figure 6 is also a close up of the same area, but it allows to perceive the upper layers of the structure as well, including the ground plane of the feeding network, one of the upper copper pads and a microstrip line.

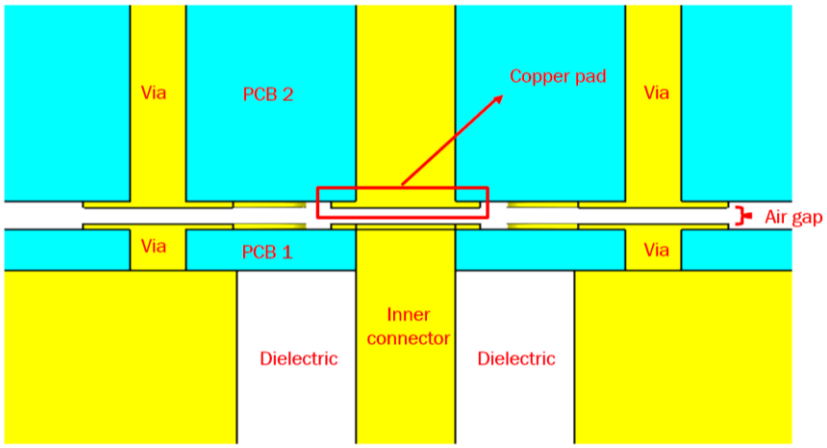

Figure 5. Close up of the cutting plane view. The area between the antenna interface and the feeding network can be appreciated.

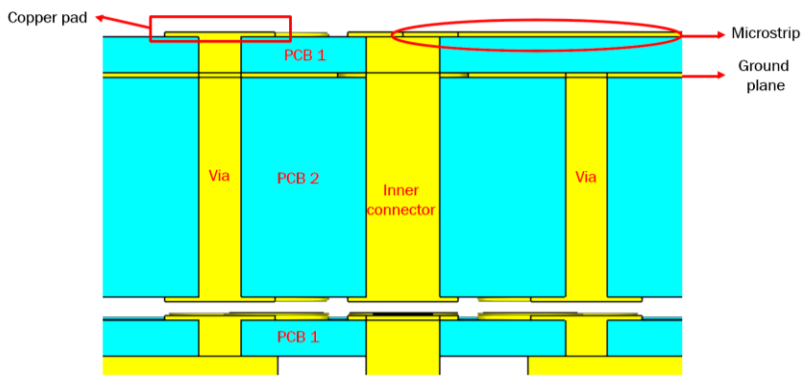

Figure 6. Close up of the cutting plane view. The upper layers of the feeding network can be appreciated.

3.1.1 Parameters and Optimization Procedure

During the design stage of the 2x2 model, some of the parameters were optimized in order to have the best performance possible within the desired frequency range of operation.

An important parameter of the model is the separation between antenna elements. This value, represented as *d,* is 7 [mm]. Such value is fixed; thus, the feeding network was designed based on it. The distance between simulation ports is twice *d*, this distance is intended to incorporate connectors to the model in a physical prototype.

The size of the air gap between conductive elements is 0.05 mm. The air gap was selected as one of the starting parameters during design, therefore the rest of the model parameters were optimized considering such value.

The thickness of the pads, the ground plane and microstrip lines is a standard manufacturing value. The microstrip lines of the feeding network and the coaxial connectors of the antenna interface were designed to work within 17-22 GHz at 50 [Ω] impedance.

The microstrip lines were shaped to connect the simulation ports to the central pads of the feeding network. The characteristics of the microstrip bends were not optimized, instead they were designed only to keep the same width along the entire length of the microstrip line.

The thickness of the different PCB layers of the model was optimized. Two different PCB layers, one thicker than the other, are used. Since there are just a few standard thickness dimensions available according to the RT5880 material datasheet (Rogers Corporation, 2021), the adjustment was limited to those values until finding a suitable combination for the model.

Finally, the following parameters were chosen using the Optimizer CST tool: copper connector radius and its pad radius, ground plane hole radius, via hole radius and its pad radius and via hole group structure radius.

Table 1 is a list of all the optimized parameters used in the 2x2 feeding network design. The parameters were slightly adjusted to match standard manufacturing dimensions, so they can be easily implemented later in a physical prototype.

Figure 7 shows some reference figures of the model for better understanding of the parameters and their descriptions and Figure 8 shows the detailed dimensions of one of the microstrip lines used in the model.

Table 1. Parameter list of the 2x2 design model.

	CST variable	Description	Value [mm]	Reference Figure 7
1	L_PCB	Thickness of PCB layer	0.254	a)
2	L_PCB1	Thickness of PCB layer	1.575	
3	L_metal	Thickness of metal layer	3	
4	L_pad	Thickness of pads, ground planes and microstrip lines	0.035	b)
5	r	Radius of copper connectors	0.2	c)
6	r_2	Radius of dielectric material in coaxial connectors	0.75	
7	r_hole	Radius of holes in ground planes	0.25	d)
8	r_vias	Radius of via holes structure	2.15	e)
9	r_pad	Radius of pads	0.5	
10	r_via_pad	Radius of via hole pads	0.6	
11	r_via	Radius of via holes	0.4	
12	LM	Partial length of microstrip line	2	f)
13	W	Width of microstrip line	0.71	
14	2d	Distance between ports, where d is the distance between two antenna elements (7 mm)	14	
15	r_blend_o	External radius of curvature of the microstrip line	1	g)
16	r_blend_i	Internal radius of curvature of the microstrip line	0.4	

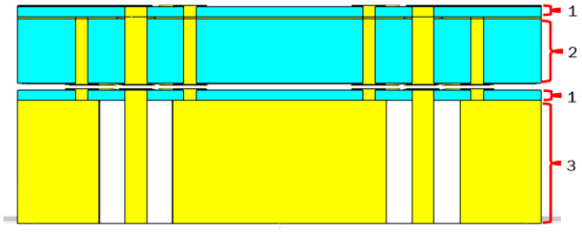

a)

Figure 7. Parameters illustration.

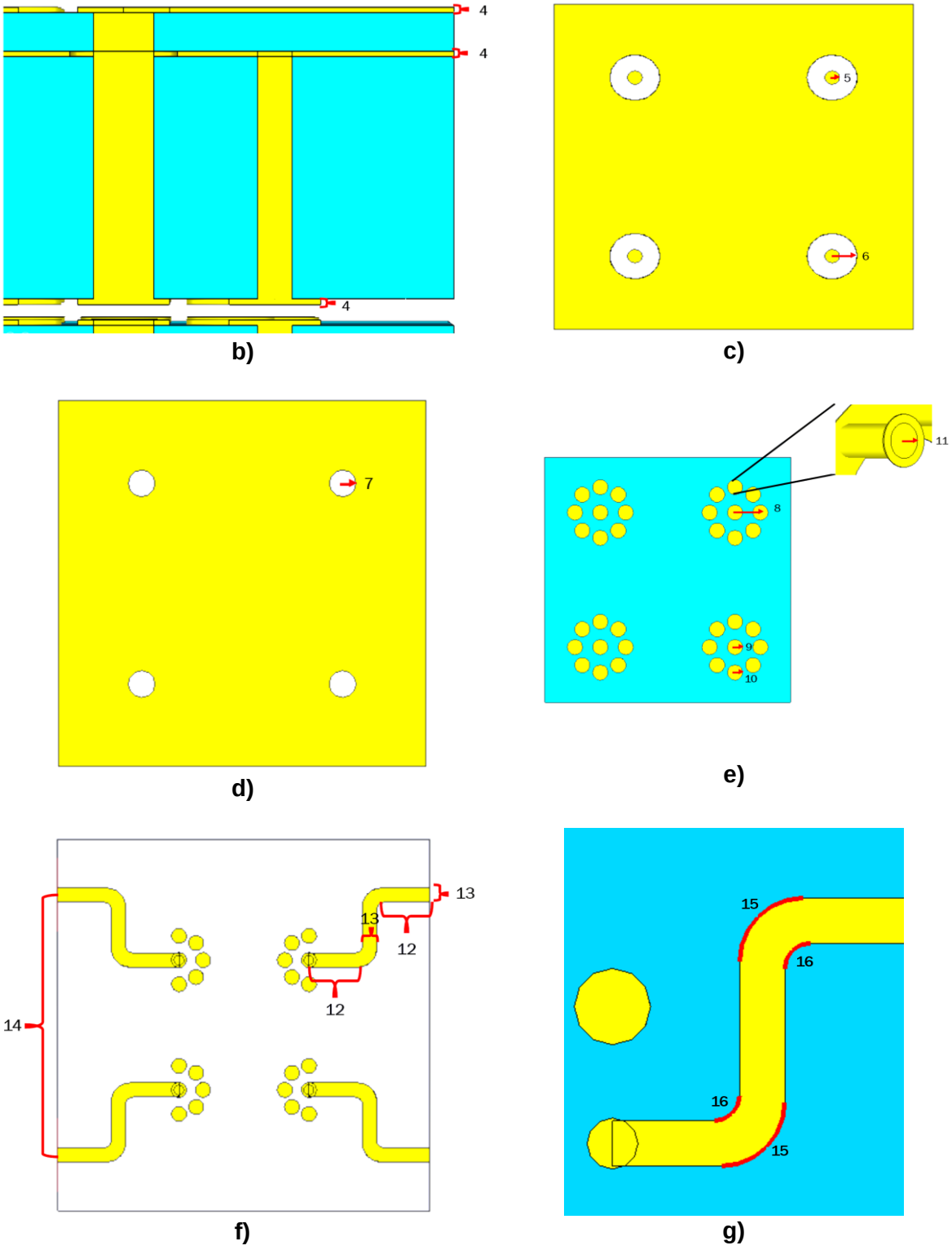

Figure 7. Parameters illustration.

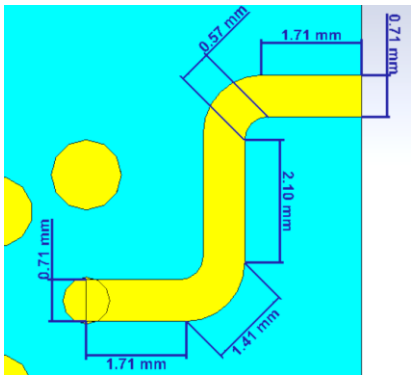

Figure 8. Microstrip dimensions.

3.2 Simulation Results of 2x2 array integration with MetaCoax

In this section, relevant results from simulations are presented, it includes the S-parameters and a back-to-back simulation of the model. The back-to-back simulation refers to the simulation of the 2x2 model with its exact copy mirrored behind.

3.2.1 S-parameters

The line impedance of all ports is near 50 Ω. Ports 1 to 4, which are the microstrip line ports, have a line impedance of around 50.3 Ω and ports 5 to 8, which are at the back of the model and belongs to the antenna interface, have a line impedance of around 54.1 Ω. The line impedances are shown in Figure 9.

The actual antenna array is designed to have an impedance of 50 Ω, so the feeding network design has to consider also that value to have a good performance and avoid impedance mismatches.

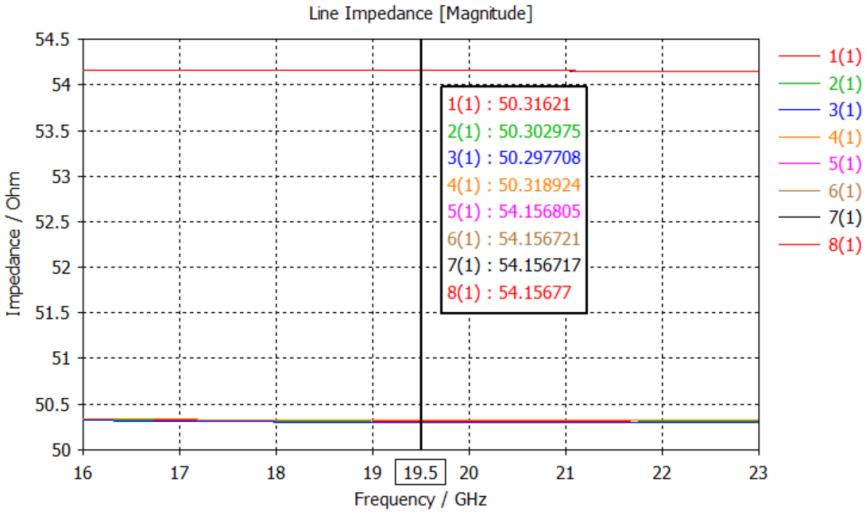

Figure 9. Line impedances of the 2x2 model.

Some of the most interesting simulation results are the S-parameters, which provide a complete description of the model by representing the relation between the voltage waves incident on the ports to those reflected from the ports.

A common way to represent the S parameters is by writing S(i,i) and S(i,j). S(i,i) is the reflection coefficient seen looking into port i when all other ports are terminated in matched loads. When a load is matched to a line, it has no reflected power. On the other hand, S(i,j) is the transmission coefficient from port j to port i when all other ports are terminated in matched loads (Pozar, 1998).

The reflection coefficient is defined as the ratio of the reflected to the incident voltage wave amplitudes and it describes how much of a wave is reflected. The transmission coefficient describes the amplitude or total power of a transmitted wave, relative to an incident wave.

In this way, in the intended frequency band where the model is having a good performance, the reflection coefficients should be low and the transmission coefficients of the input ports to their respective output ports should be high.

All input ports of the 2x2 model are Ports 1 to 4 and they are designed with the same geometry. Thus, it is presented here some relevant results of ports 3 and 7 as an example. In Figure 10, the input port 3 and the output port 7 of the model are highlighted.

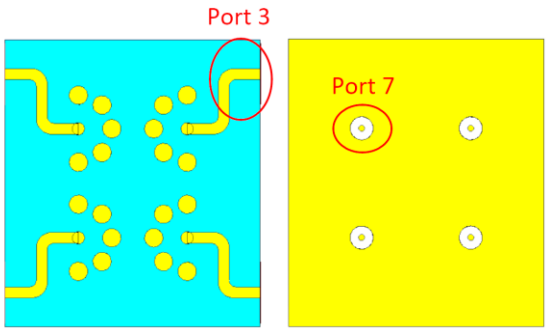

Figure 10. Input port 3 and output port 7 of the 2x2 model.

The transmission coefficient or parameter S(7,3) is illustrated in Figure 11. S(7,3) parameter is above -1 dB over 17-22 GHz and it has a peak of around -0.4 dB near the central frequency 19.5 GHz. The reflection coefficient or parameter S(3,3) is illustrated in Figure 12. S(3,3) parameter is below -10 dB over 17-22 GHz and it has a trough of around -28 dB near the central frequency 19.5 GHz.

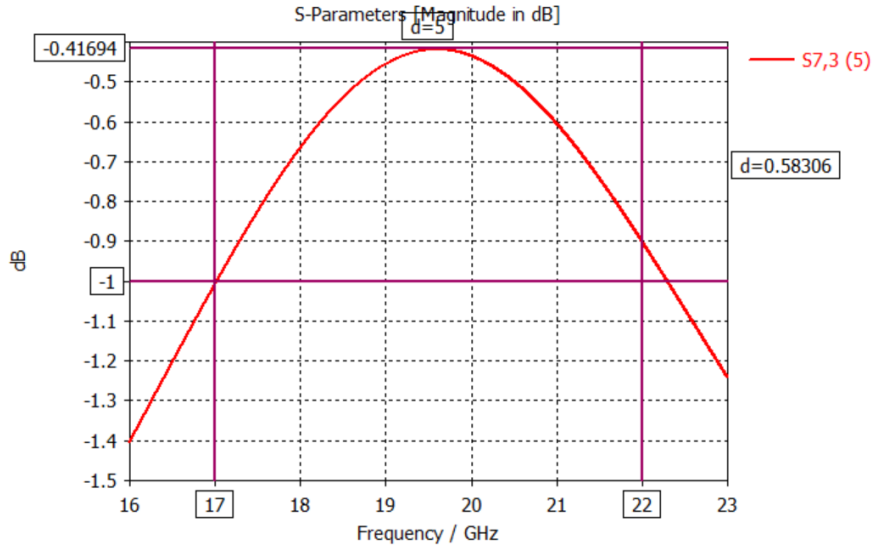

Figure 11. S(7,3) parameter in dB.

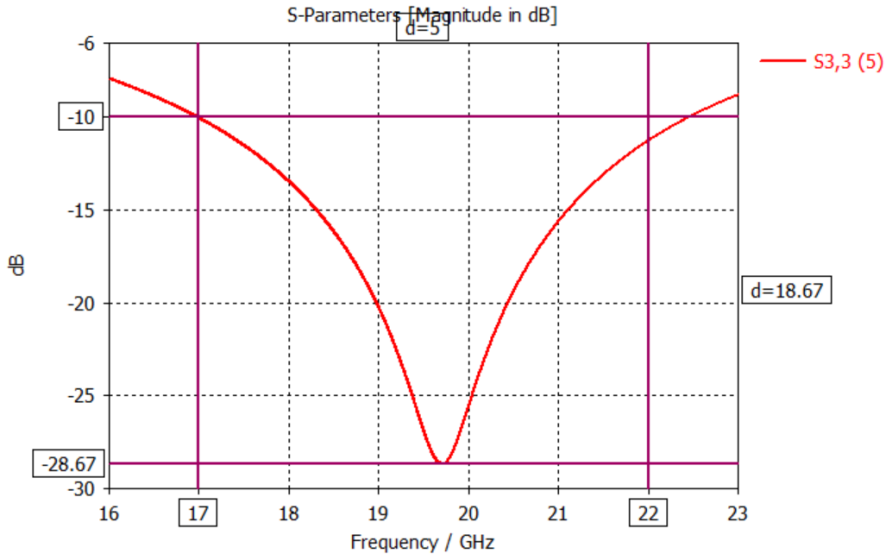

Figure 12. S(3,3) parameter in dB.

Both S(7,3) and S(3,3) parameters are shown in the same graph in Figure 13. Mutual coupling among all ports is below -50 dB, as illustrated in Figure 14.

The simulation results of the 2x2 model presented in this thesis project, are similar to the ones observed during preliminary test of the full contactless MetaCoax technology. In preliminary tests of the technology without optimization procedures, it was observed a transmission coefficient above -1.5 dB, a reflection coefficient below -8 dB and a mutual coupling between two ports below -50 dB over 22-42 GHz.

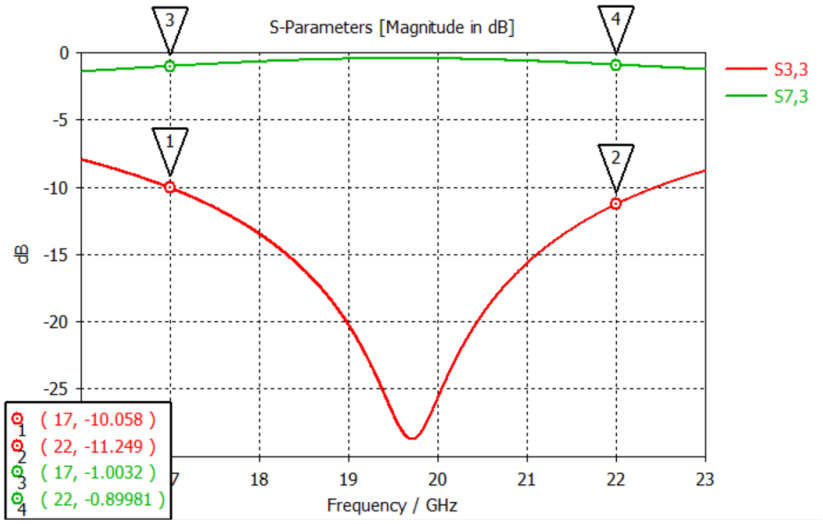

Figure 13. Transmission and reflection coefficients of the 2x2 model.

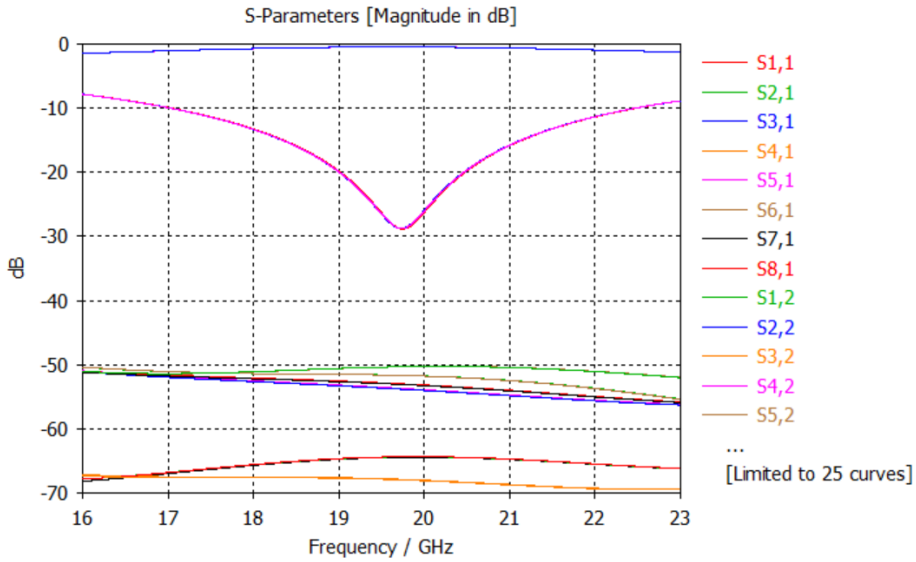

Figure 14. S parameters of the 2x2 model.

3.2.2 Back-to-back simulation

For the back-to-back simulation, an exact copy of the 2x2 feeding network model was positioned behind it. In this test, the antenna interface layers are not used. Figure 15 shows the back-to-back configuration.

Figure 16 shows the S(7,3) and S(3,3) parameters found with the back-to-back test. The peak and trough of the transmission and reflection coefficients respectively, are located around 16.5 GHz in this case. This behavior may be due to the reflections and standing waves that were created by “extending” the transmission lines of the model, since during the back-to-back test the signal has to travel twice through the feeding network model.

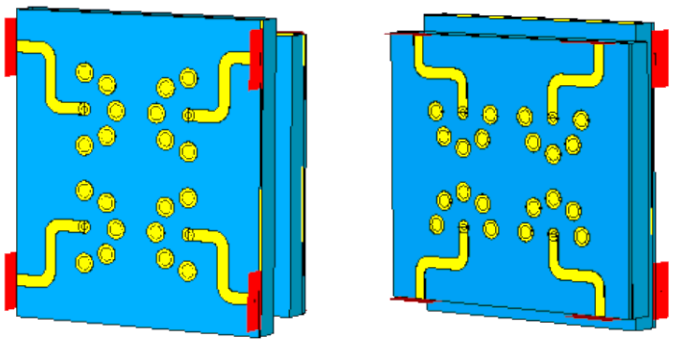

Figure 15. Back-to-back configuration of the 2x2 model: front (left) and back (right).

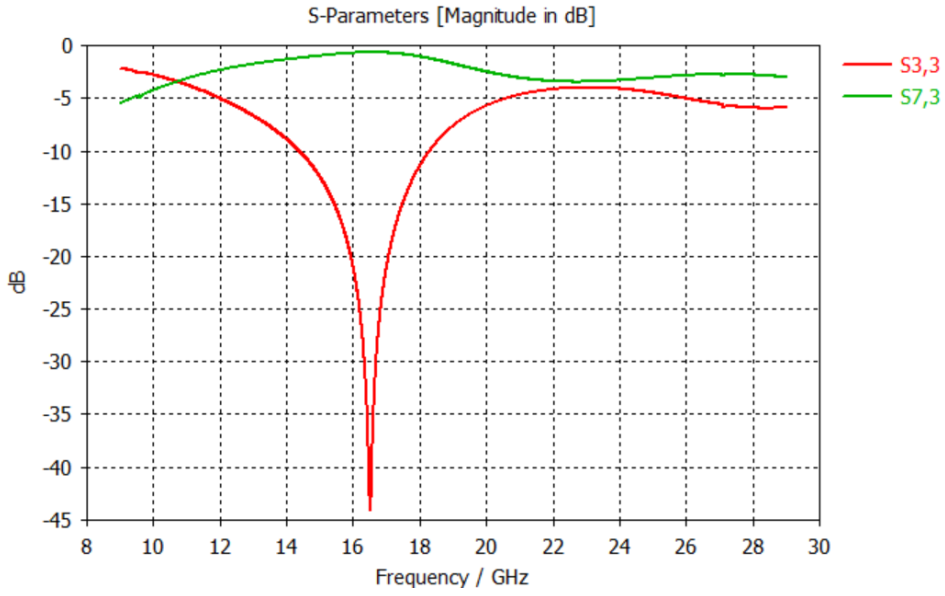

Figure 16. S parameters of the 2x2 model back-to-back test.

3.3 Design and model of 4x4 array integration with MetaCoax

After designing and testing the 2x2 feeding network, the next step was extending it to a 4x4 model. This new version required more layers, some changes respecting the shapes and sizes of the microstrip lines of the model and another optimization procedure for its different components, such as via hole dimensions, inner connectors and pads. Figure 17 shows the main parts of the 4x4 feeding network design.

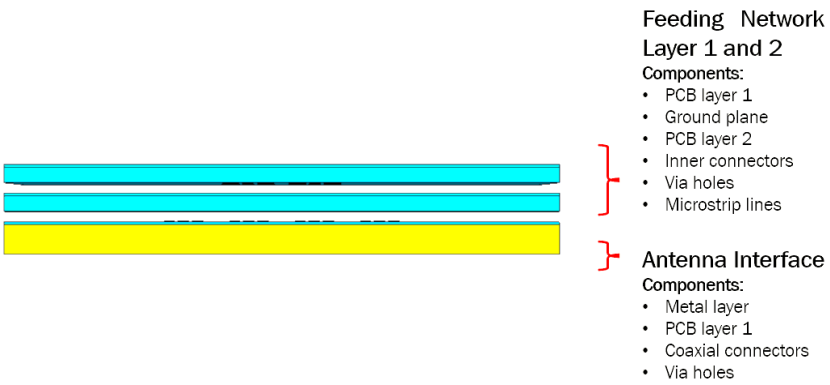

Figure 17. 4x4 model structure.

The 4x4 feeding network model can be divided in two sections, each section has two PCB layers, a ground plane, connectors, via holes, pads and microstrip lines. The antenna interface has a metal layer, a PCB layer, coaxial connectors, via holes and pads. In this case, there is an air gap between each section of the feeding network and also between the feeding network and the antenna interface.

The material of the PCB layers is Rogers RT5880. The metal and ground planes, vias, pads, connectors and microstrip lines were modeled with copper. The dielectric material used in the antenna interface for the coaxial connector is PTFE.

Copper connectors with dielectric PTFE coaxials were added to the 4x4 model. Their geometry is shown in Figure 18.

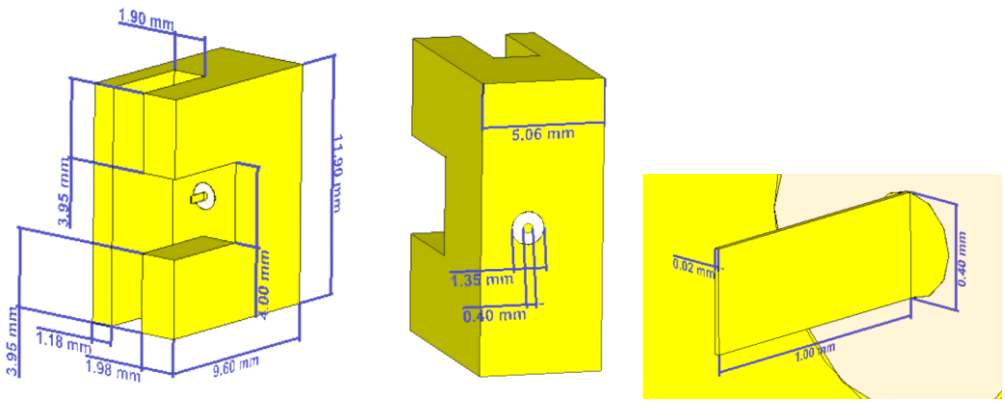

Figure 18. Copper connector geometry.

The copper connectors are attached to the end of each microstrip line as shown in Figure 19. In this figure, the front and the back of the feeding network are shown.

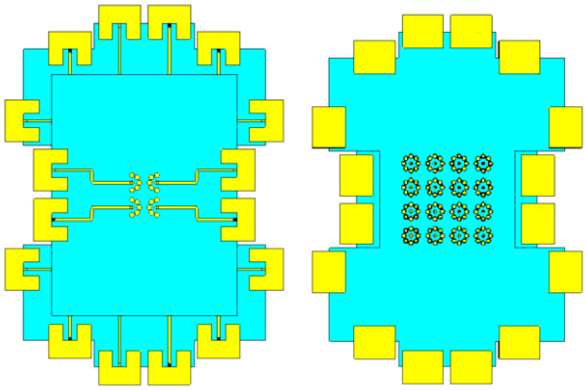

Figure 19. Front (left) and back (right) of the 4x4 feeding network.

As mentioned before, the feeding network has two main sections, the upper layer is designed to feed four ports and the lower layer is designed to feed 12 ports. The upper layer is illustrated in Figure 20 and the lower layer in Figure 21. Both sections of the feeding network are designed to have a mirror type geometry and the whole integration board feeds 4 ports per side.

The 4x4 model continues using mushroom-like electromagnetic band-gaps around each inner connector.

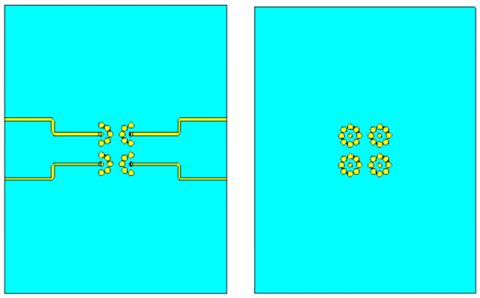

Figure 20. Front (left) and back (right) of the 4x4 feeding network upper section.

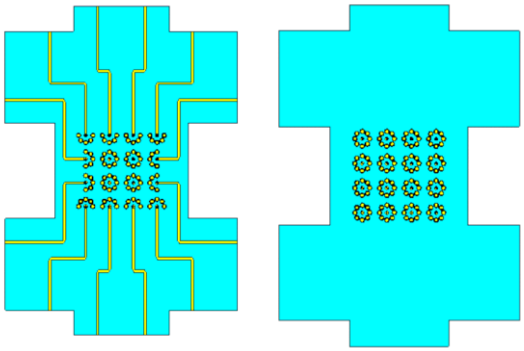

Figure 21. Front (left) and back (right) of the 4x4 feeding network lower section.

The antenna interface, which in this case has 16 output ports, is shown in Figure 22. The dimensions of all PCB layers and ground planes were adjusted, so the copper connectors could fit.

Finally, in Figure 23 there are two images of the designed feeding network attached to the antenna interface. In this model, the input ports for simulation are placed at the dielectric coaxials of the copper connectors which appear in red in Figure 24.

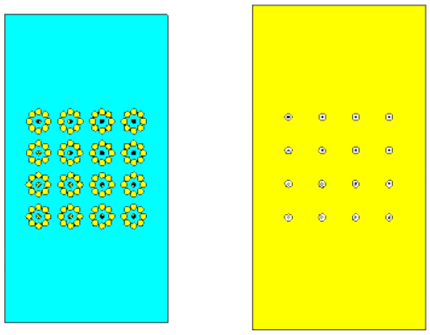

Figure 22. Front (left) and back (right) of the antenna interface.

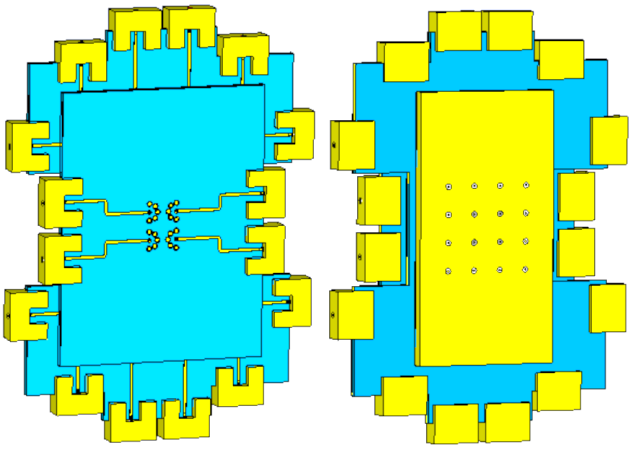

Figure 23. Front (left) and back (right) of the 4x4 model.

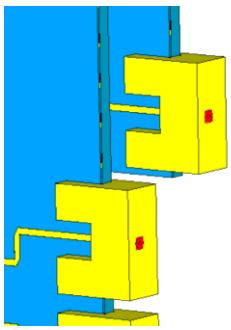

Figure 24. Two copper connectors with their input ports (in red) for simulation.

Figure 25. shows the cutting plane view of the 4x4 model. In this image there are some of the via holes, coaxial connectors and air gaps between sections.

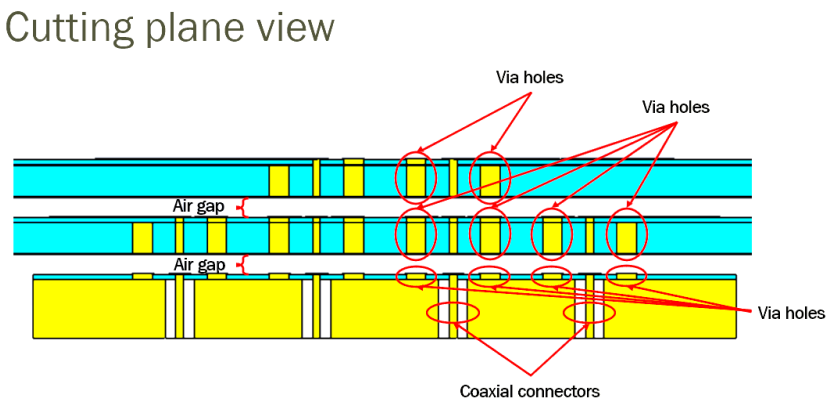

Figure 25. Cutting plane view of the 4x4 feeding network model.

Figure 26 is a close up of the cutting plane view. In this model, the air gap is the space between copper pads. During the design stage, an air gap of 0.05 mm was considered.

In Figure 26, there are some of the via holes made for stopping leakage and mutual coupling, inner connectors, copper pads, a ground plane, the different PCB layers and a microstrip line. This first close up is a detailed image of the lower section of the feeding network which connects one input port with the antenna interface.

Figure 26. Close up of the cutting plane view. The area between the antenna interface and the lower layer of the feeding network can be appreciated.

Figures 27 and 28 are also close ups of the cutting plane view. Figure 27 is a detailed image of the lower section of the feeding network, but unlike Figure 26, this section allows to connect the upper layer with the antenna interface. Figure 28 illustrates a part of the feeding network that connects the upper and lower layers of the model.

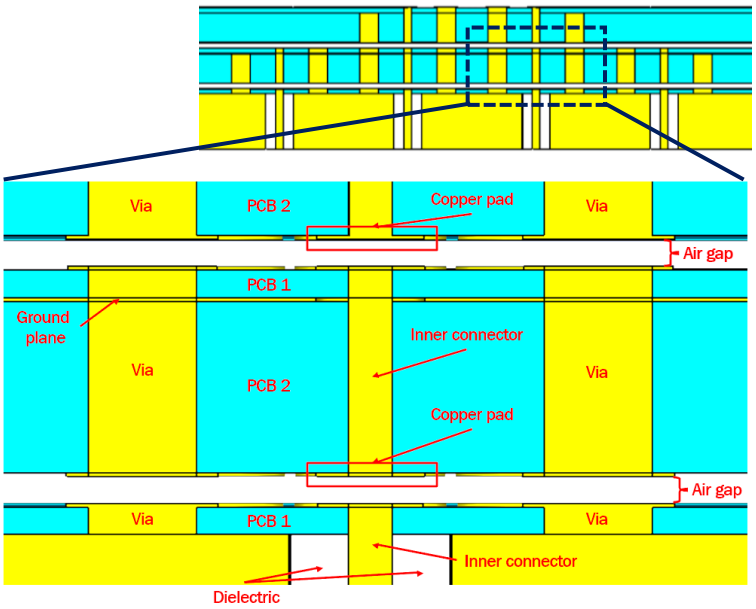

Figure 27. Close up of the cutting plane view. The area that connects the upper and lower layers of the feeding network with the antenna interface can be appreciated.

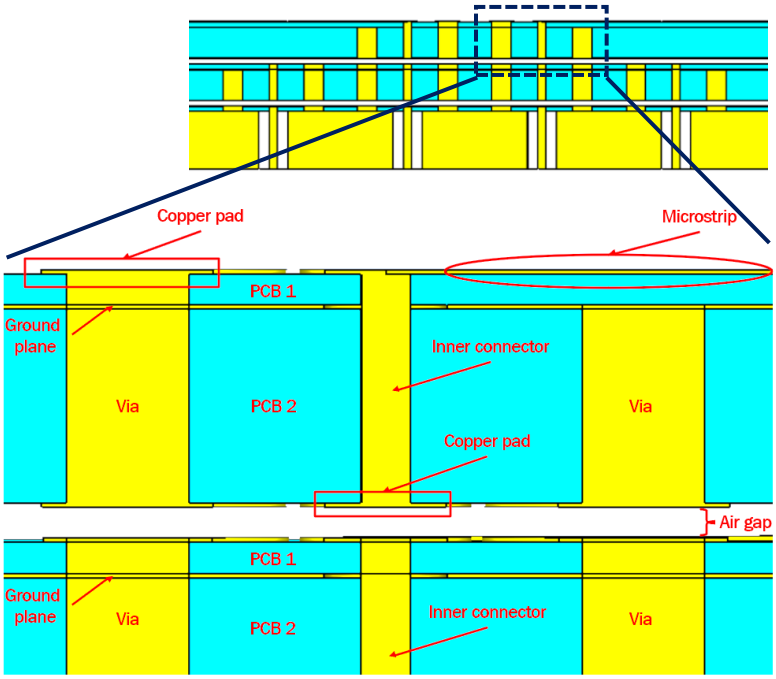

Figure 28. Close up of the cutting plane view. The area between the upper and lower layers of the feeding network can be appreciated.

3.3.1 Parameters and Optimization Procedure

During the design of the 4x4 feeding network, some parameters were optimized in order to have a good performance for all the ports over the frequencies 17-22 GHz.

The separation between antenna elements is still 7 mm and the distance between simulation ports is 14 mm.

The size of the air gap between conductive elements is also 0.05 mm in this model. The air gap was selected as one of the starting parameters during design, therefore the rest of the model parameters were optimized considering such value. After completion of the model, the effects of changing the air gap dimension were studied.

The thickness of the pads, ground planes and microstrip lines is 0.035 mm. The microstrip lines of the feeding network and coaxial connectors of the antenna interface were designed to work within 17-22 GHz at approx. 50 [Ω] impedance.

The microstrip lines were shaped to connect the copper connectors to the central pads of the feeding network. The microstrip lines on the lower layer of the feeding network have a length of approx. 40 mm and the microstrip lines on the upper layer have a length of approx. 25 mm. The lengths of the different microstrip lines were adjusted in order to have a similar phase in all the ports.

The characteristics of the microstrip bends were optimized and are slightly different from the ones used in the 2x2 feeding network model. The microstrip lines bends looks like the one shown in Figure 29. The bend has a chamfer width of 0.9 mm at an angle of 30°.

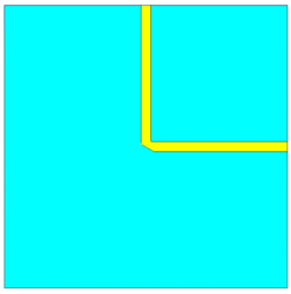

Figure 29. Microstrip line bend with a chamfer.

The optimized characteristics of the bends were found by creating simple microstrip line models, as shown in Figure 30. The three microstrip lines had approx. the same length, the first one is a straight line, the second microstrip has a bend of 90° with rounded edges and the third microstrip line has also a bend of 90° but with a chamfer.

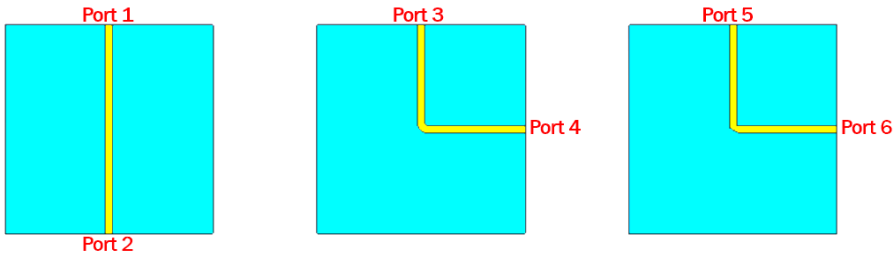

Figure 30. Models for microstrip line bends optimization.

The last microstrip line was modified until having a good transmission and reflection coefficient. Figure 31 shows the final S parameters of the three models. The graphs show that the microstrip line with a chamfer has a better performance than the microstrip line with rounded edges. The straight microstrip line was simulated just as a reference and it has the best performance among the three models as expected.

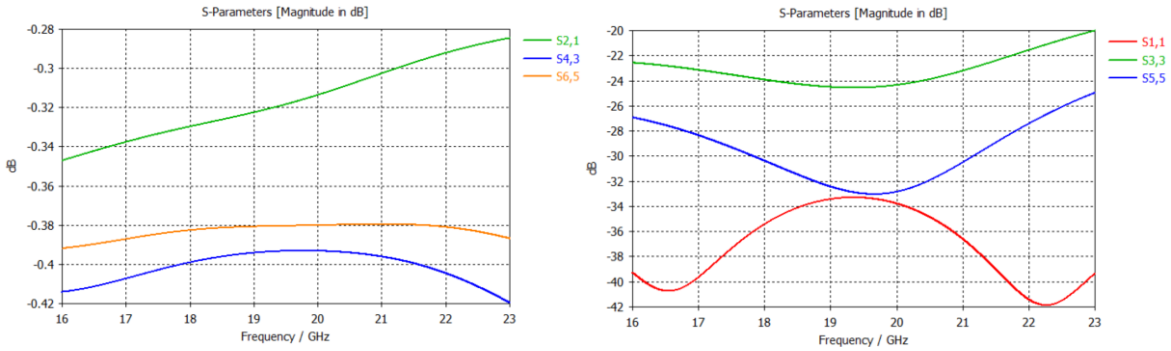

Figure 31. Transmission coefficients (left) and reflection coefficients (right) of the microstrip line models.

In this model, PCB layers with two different thickness values are used. The thickness values were selected from the available standard dimensions (Rogers Corporation, 2021). Several combinations were tested until finding the most suitable for the model.

Some parameters were optimized using the Optimizer CST tool or changing manually their values to match standard manufacturing dimensions, so they can be implemented later in a physical prototype. The parameters that followed such optimization procedure are: the copper connector radius and its pad radius, via hole radius and its pad radius and the via hole group structure radius.

Table 2 is a list of all the optimized parameters used in the 4x4 integration network design and Figure 32 shows reference figures of the model for better understanding of the parameters and their description.

Table 2. Parameter list of the 4x4 feeding network model.

	CST variable	Description	Value [mm]	Reference Figure 32
1	L_PCB	Thickness of PCB layer	0.254	a)
2	L_PCB1	Thickness of PCB layer	1.575	
3	L_metal	Thickness of metal layer	3	
4	L_pad	Thickness of pads, ground planes and microstrip lines	0.035	b)
5	r	Radius of copper connectors	0.2	c)
6	r_2	Radius of dielectric material in coaxial connectors	0.75	
7	r_hole	Radius of holes in ground planes	0.5	d)
8	r_vias	Radius of via holes structure	2.1	e)
9	r_pad	Radius of pads	0.5	
10	r_via_pad	Radius of via hole pads	0.7	
11	r_via	Radius of via holes	0.5	f)
12	LM_port1	Partial length of microstrip line (Port 1 in test)	11	g)
13	LM_port2	Partial length of microstrip line (Port 2 in test)	18.7	h)
14	LM_port3	Partial length of microstrip line (Port 3 in test)	15	
15	LM_port4	Partial length of microstrip line (Port 4 in test)	6	
16	LM_port4_1	Partial length of microstrip line (Port 4 in test)	17	
17	W	Width of microstrip line	0.7	i)
18	2d	Distance between ports, where d is the distance between two antenna elements (7 mm)	14	
19	width_o	Chamfer width of microstrip lines	0.9	j)
20	angle_o	Chamfer angle of microstrip lines	30°	

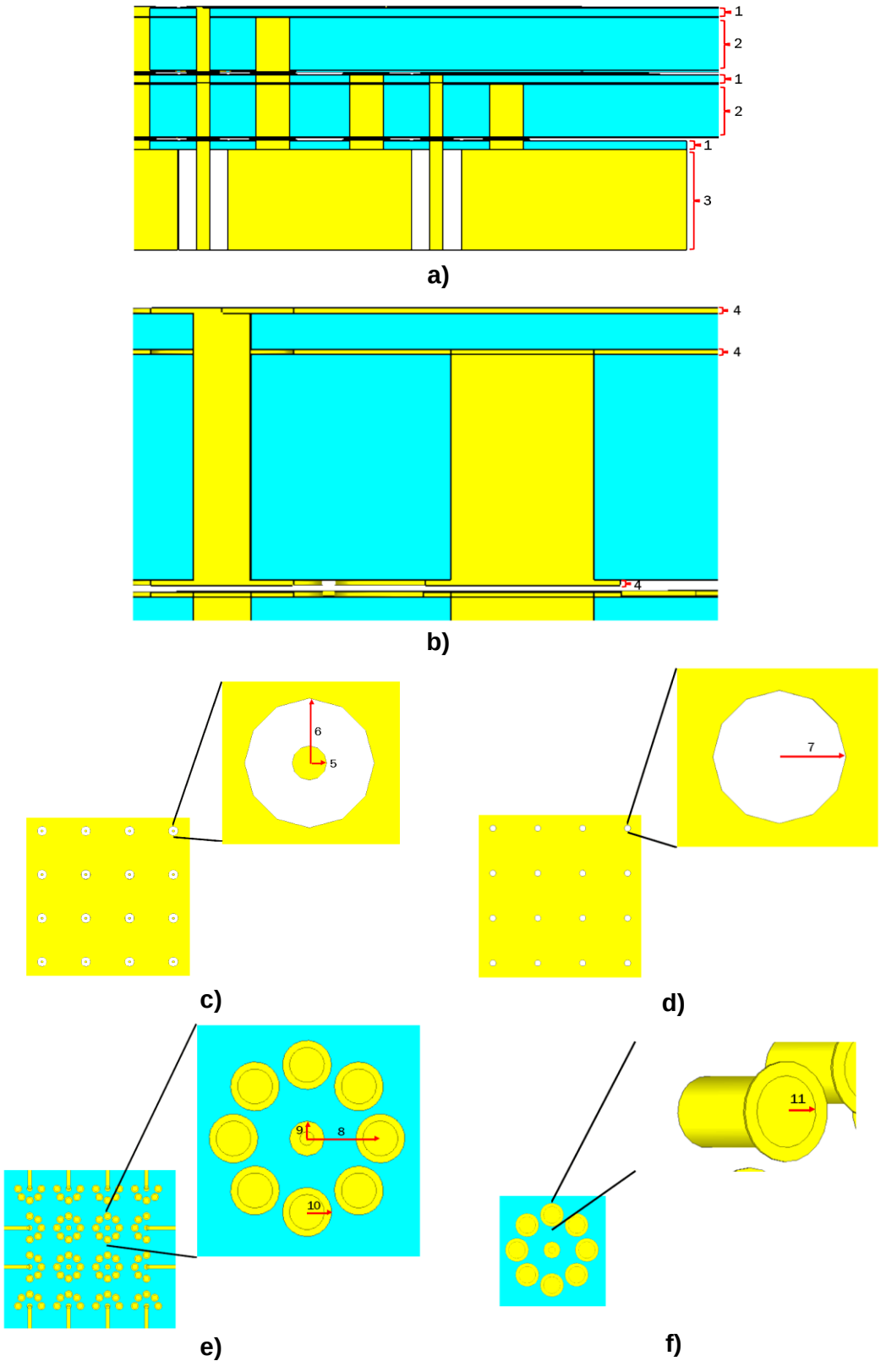

Figure 32. 4x4 model: parameter illustrations.

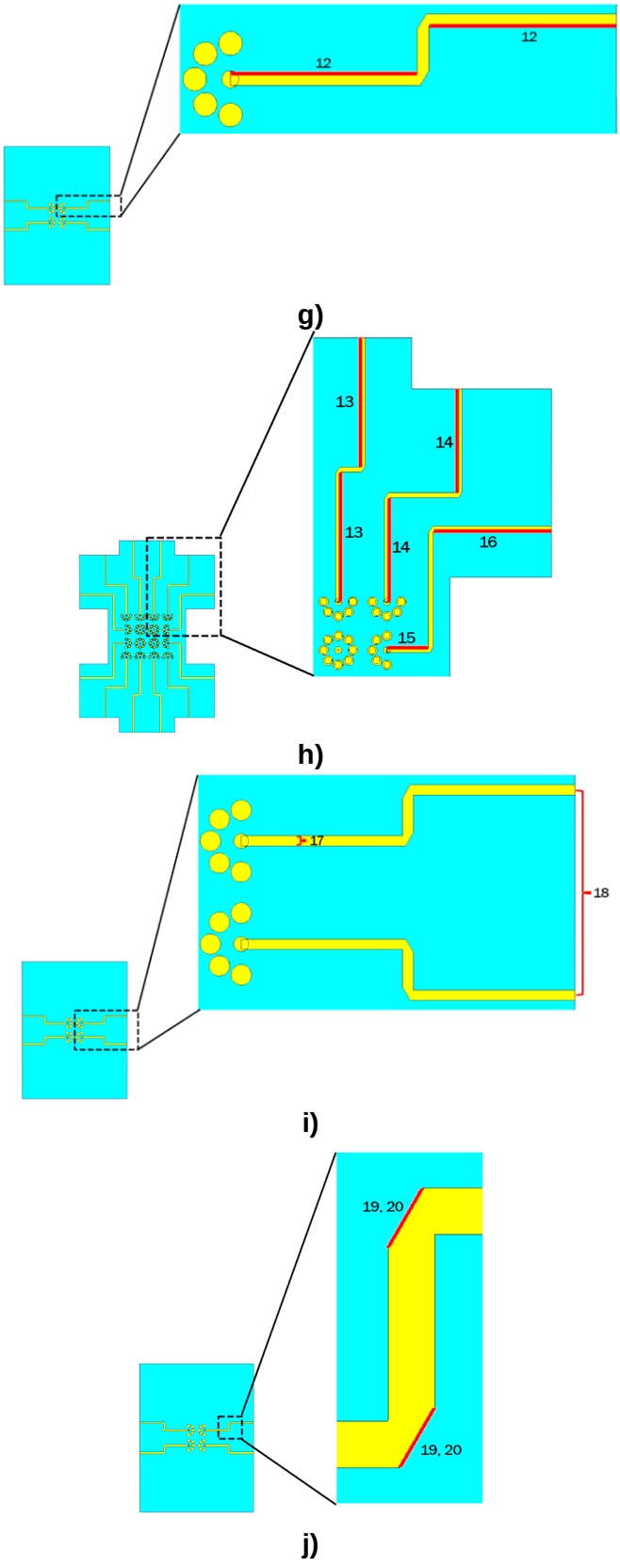

Figure 32. 4x4 model: parameter illustrations.

3.4 Simulation Results of 4x4 array integration with MetaCoax

In this section, relevant results from simulations are presented, it includes the S-parameters, a back-to-back simulation of the model and misalignment tests. Back-to-back refers to the simulation of the 4x4 model with its exact copy mirrored behind. The misalignment tests are simulations of the 4x4 model with some layers in different positions. More details of each test and their results are presented in this section.

3.4.1 S-parameters

The model is designed to have symmetry along x and y axis, as illustrated in Figure 33. In this way, it was possible to test and study the ports that belong to one quadrant of the model, since the rest of them have exactly the same performance. The four input ports that were mainly tested in this thesis are indicated in Figure 34.

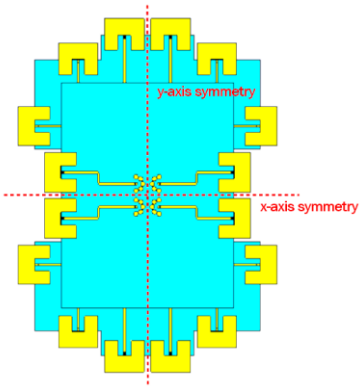

Figure 33. Symmetry axes in the 4x4 model.

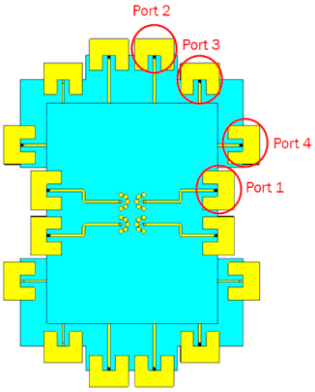

Figure 34. Port definition of the 4x4 model.

The transmission coefficients S(5,1), S(6,2), S(7,3) and S(8,4) of the model are shown in Figure 35. It can be seen that all transmission coefficients are above -1.4 dB within the frequency range 17-22 GHz. The reflection coefficients S(1,1), S(2,2), S(3,3) and S(4,4) of the model are illustrated also in Figure 35. The reflection coefficients are below -10 dB within 17-22 GHz. Plots of each transmission and reflection coefficients separately can be found in the Annex.

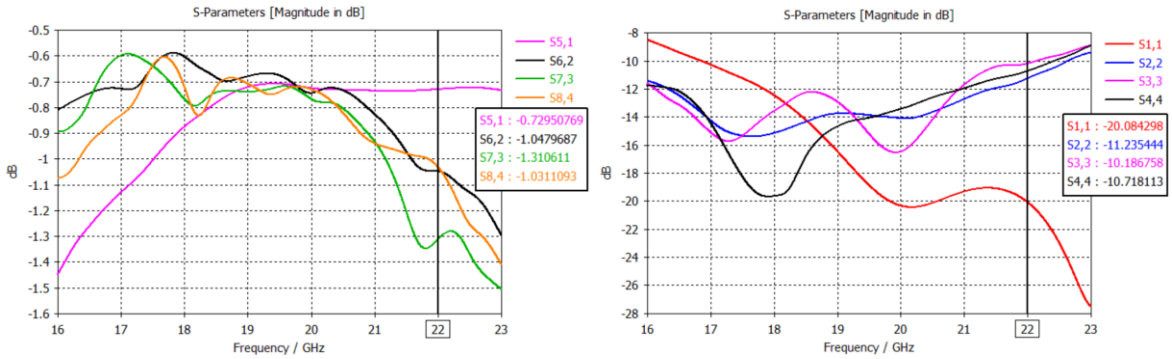

Figure 35. Plots of transmission (left) and reflection (right) coefficients of the model.

Mutual coupling among all ports is below -30 dB, as illustrated in Figure 36. Figure 36 also shows the same plots but in linear scale, where the transmission and reflection coefficients can be appreciated, as well as the mutual coupling of the model.

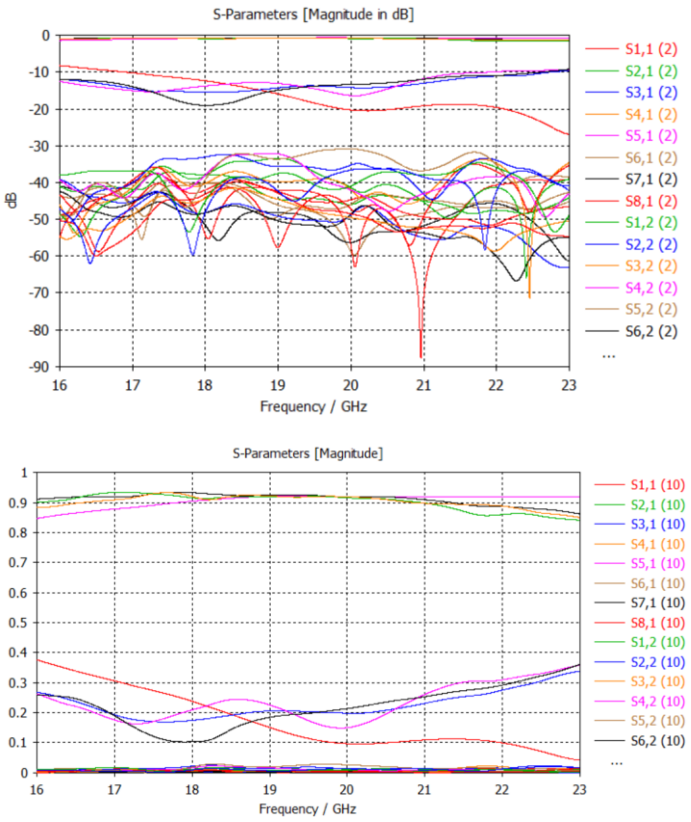

Figure 36. S-parameters of the model in dB (up) and in linear scale (down).

3.4.2 Back-to-back simulation

For the back-to-back simulation, an exact copy of the 4x4 feeding network model was positioned behind it and then rotated 90°. In this test, the antenna interface layers are not used. In this case and similarly to the previous tests of the 4x4

model, only the ports located in one quadrant of the model were tested, since the model has symmetry along x and y axes. Figure 37 shows the back and front of the back-to-back configuration.

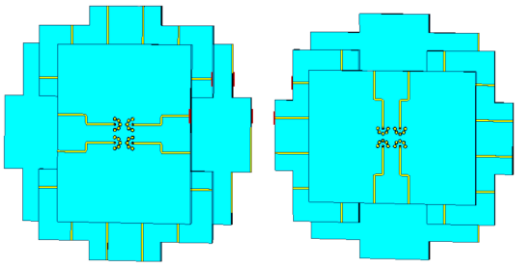

Figure 37. Back-to-back configuration of the 4x4 model: front (left) and back (right).

Figure 38 shows the transmission and reflection coefficients of this configuration. The peak and trough of all transmission and reflection coefficients respectively, are located within 16 to 16.5 GHz. The performance of the model during this test was similar to the one observed in the 2x2 model. Figure 39 shows both coefficients in the same plot.

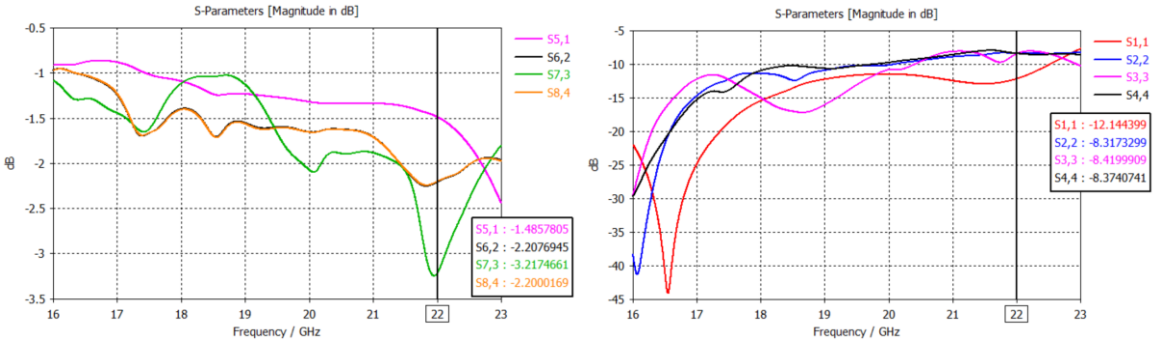

Figure 38. Transmission (left) and reflection (right) coefficients of the back-to-back configuration of the 4x4 model.

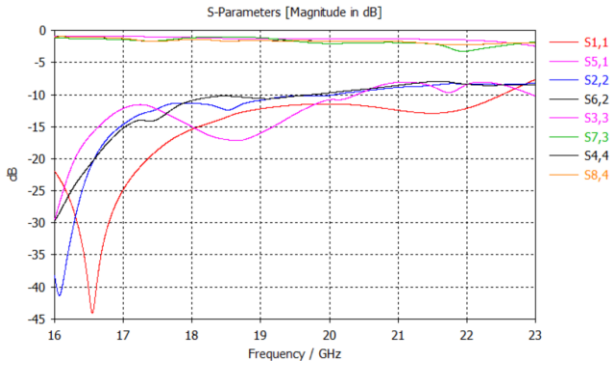

Figure 39. S-parameters of the back-to-back configuration of the 4x4 model.

3.4.3 Misalignment tests

Misalignment tests were performed on the 4x4 integration model in order to know more about its performance under possible manufacturing error conditions. The misalignment was tested along x, y and z axis.

The x and y misalignments were tested by moving the upper layer of the feeding network and the antenna interface, as illustrated in Figure 40. In Figure 40, dx and dy refer to the different positions of misalignment in which the model was tested, such positions were from 0 to 0.2 mm in both directions. The maximum tested misalignment is almost 50% of the radius of the pads in the model, which is equal to 0.5 mm.

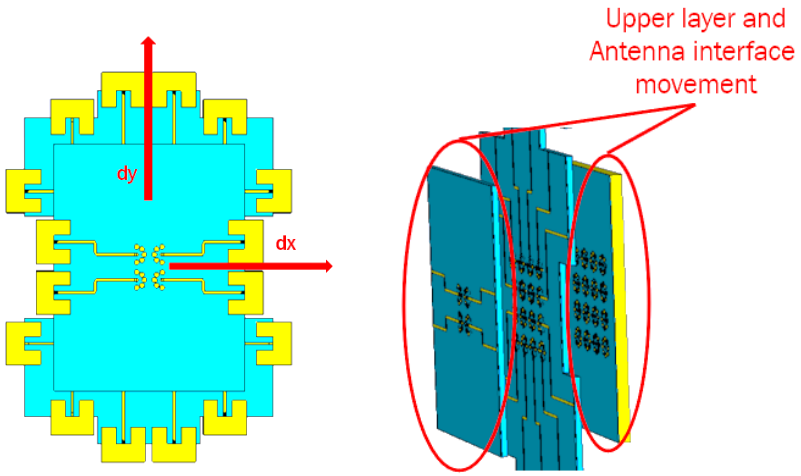

Figure 40. Motion directions for misalignment tests (left) and illustration of the layers used to simulate it (right).

Figure 41 shows a perspective view of the copper connectors and pads of the model as well as their front view when there is no misalignment. On the other hand, Figure 42 shows the perspective view of the copper connectors and their pads during misalignment scenarios. In this figure, the front views illustrate movements of 0.1 and 0.2 in x-axis and y-axis directions.

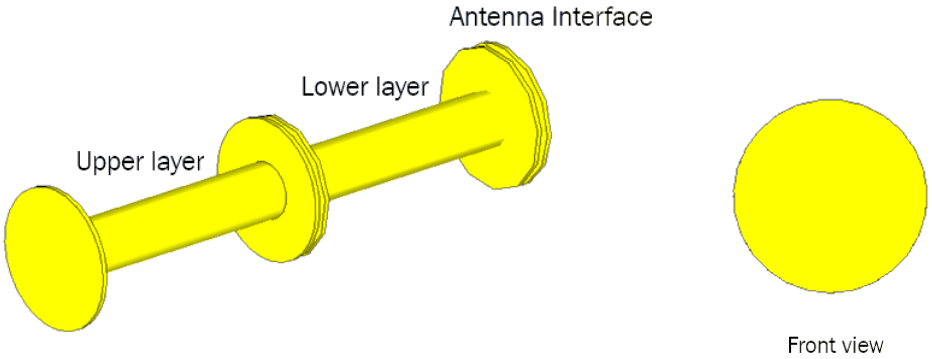

Figure 41. Views of copper connectors and pads under no misalignment conditions.

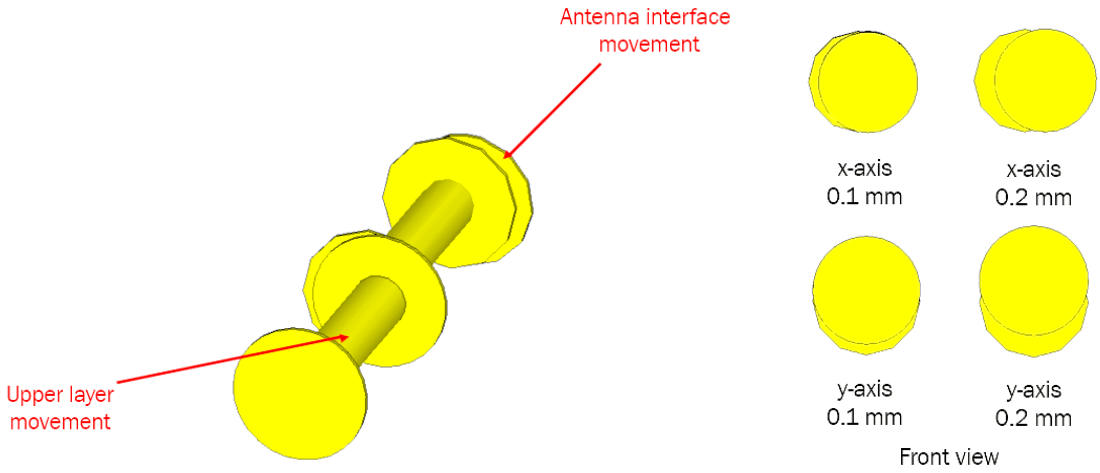

Figure 42. Views of copper connectors and pads under some misalignment conditions.

On the other hand, the z axis misalignment was studied by changing the air gap parameter in simulations. The feeding network model was designed to have a 0.05 mm air gap between layers, but during manufacturing this value could differ. Just three air gap values were tested during simulations, 0 mm with direct contact of copper pads, 0.05 mm and 0.1 mm.

Figure 43 show the transmission coefficient from port 1 to port 5. In this plot it can be seen that a misalignment value of 0.1 mm in x and no misalignment in y, is the same of having no misalignment in x and a misalignment of 0.1 mm in y.

Also, the transmission coefficient values from port 1 to port 5 under no misalignment conditions are above -1.1 dB over 17-22 GHz, it dropped to -1.2 dB with misalignment conditions along x or y axis and it dropped again to -1.3 dB under misalignment conditions along x and y axes combined. So, having a misalignment in both directions at the same time, is roughly twice the effect on the model of a misalignment in only one direction at lower frequencies.

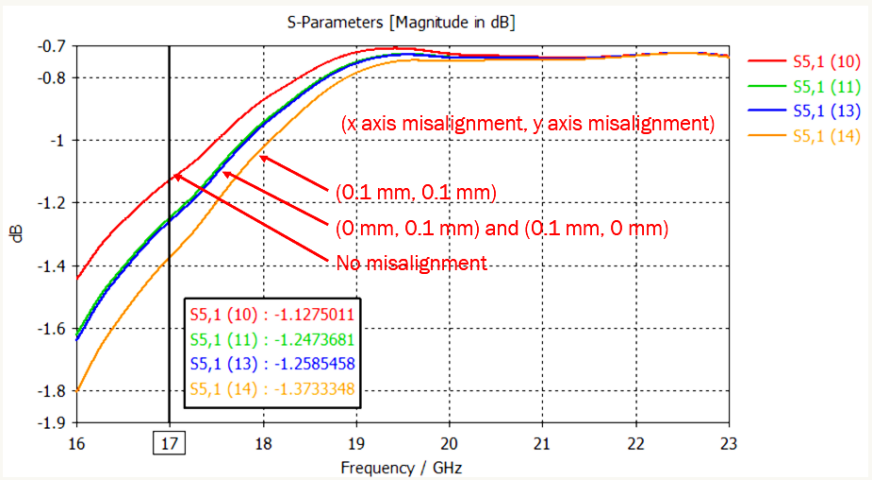

Figure 43. Transmission coefficient from port 1 to 5 under x and y misalignment conditions.

The reflection coefficient of port 1 has similar effects under misalignment conditions. Figure 44 shows the corresponding plots.

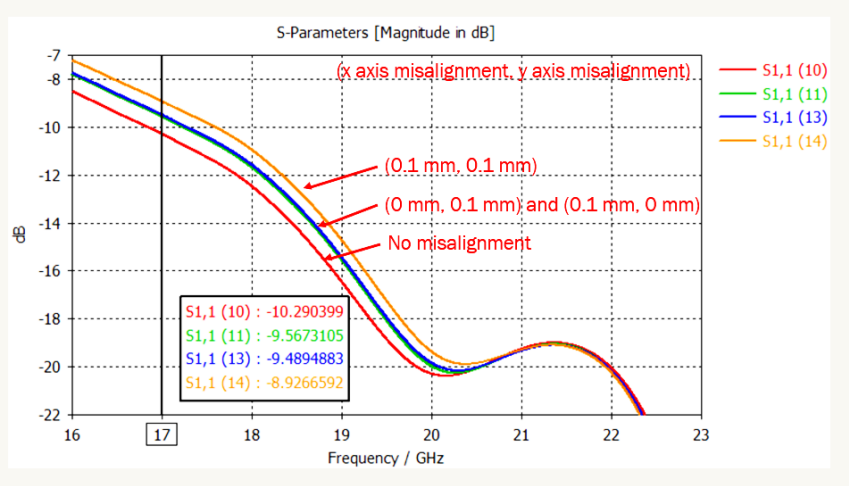

Figure 44. Reflection coefficient of port 1 under x and y misalignment conditions.

Figure 45 show the corresponding comparison of the transmission coefficients from port 1 to 5 when applying misalignment values along x and y axes from 0.1 mm to 0.2 mm. And Figure 46 show the reflection coefficient of port 1 under the same conditions.

Port 1 performance was the most affected during the misalignment tests, that is the reason of presenting the corresponding plots in this section. It has transmission coefficient values above -1.1 dB over 17-22 GHz with no misalignments and transmission coefficient values above -2 dB over the same frequency range under the maximum tested misalignment conditions along x and y axis at lower frequencies. On the other hand, the reflection coefficient went from values below -10.2 dB to -6.6 dB.

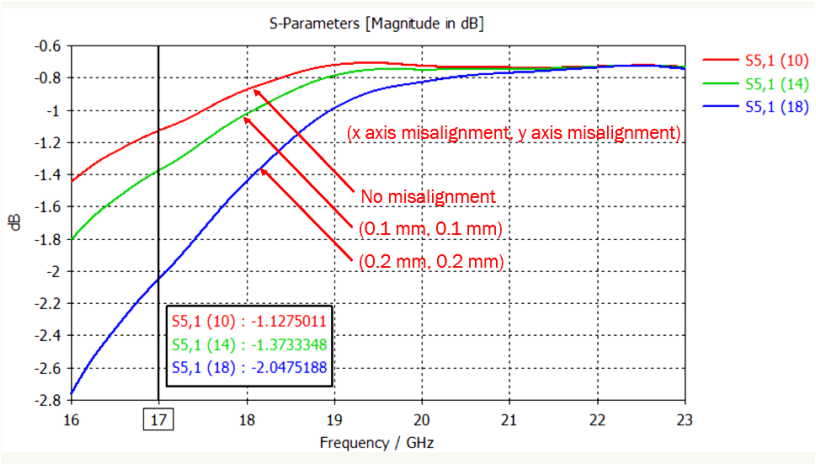

Figure 45. Transmission coefficient from port 5 to port 1 under maximum tested x and y misalignment conditions.

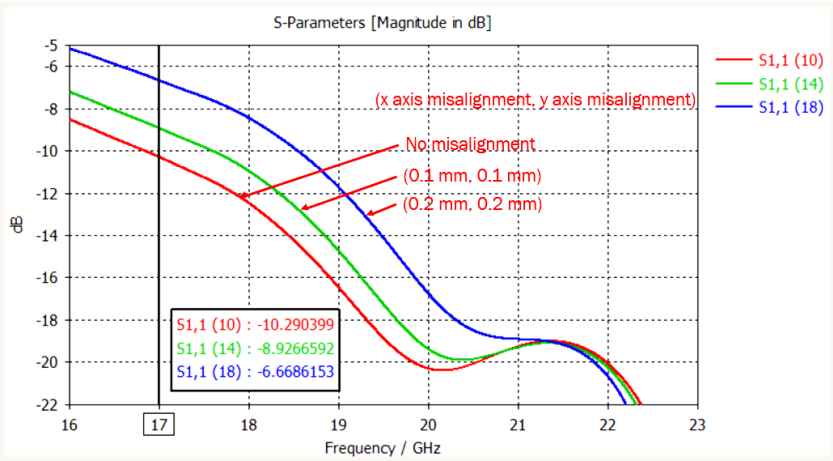

Figure 46. Reflection coefficient of port 1 under maximum tested x and y misalignment conditions.

During misalignment tests along z axis, the air gap between copper pads was changed to study its effects on the model performance. Increasing the gap had an effect on the model's bandwidth as shown in Figures 47 and 48.

In such figures, it can be appreciated that the operation bandwidth of the model moves to higher frequencies as the size of the gap increases. Also, it seems that the coupling increases with smaller gaps. Plots of the performance of ports 1 to 4 under variations of the air gap in dB and linear scale can be found in the Annex.

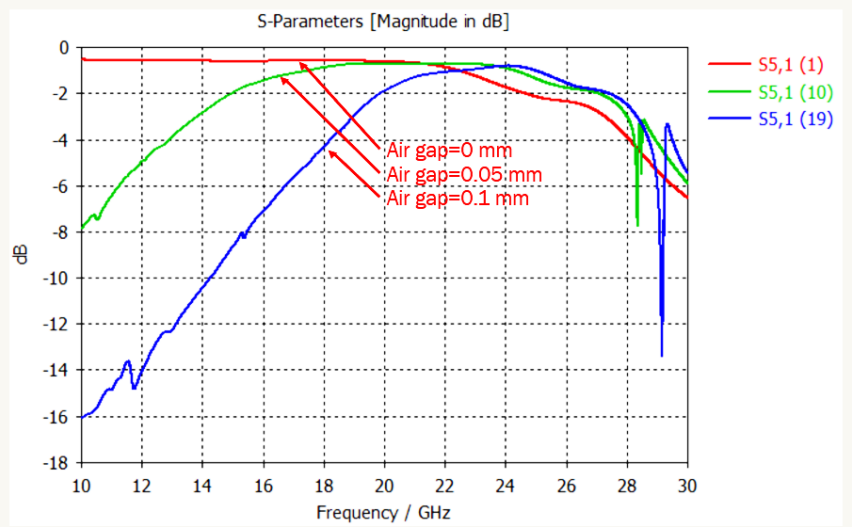

Figure 47. Transmission coefficient from port 1 to 5 with different air gap values.

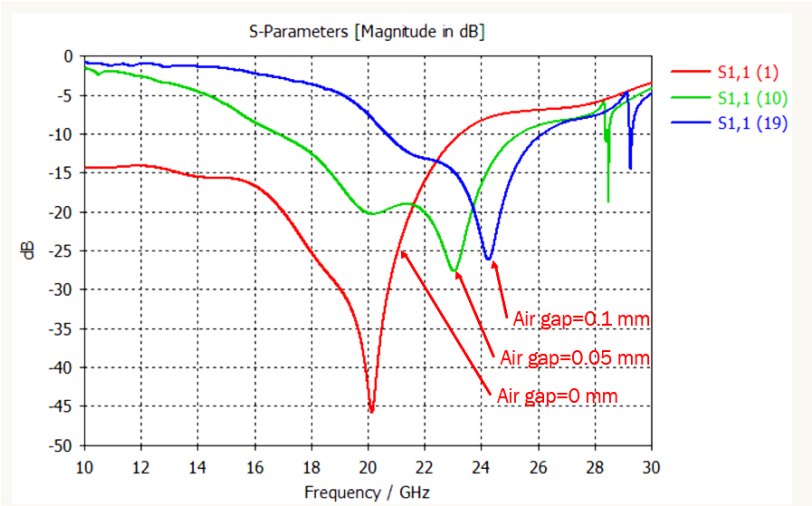

Figure 48. Reflection coefficient of port 1 with different air gap values.

3.5 Design and model of 4x4 array integration with MetaCoax and bonding layers

Having in mind a future physical prototype of the integration model, whose design implies having a gap in between PCB layers, is important to consider different manufacturing processes options.

One way to create the gaps for the 4x4 model is by using screws and adjusting the gap. Nevertheless, another possible option is using an adhesive layer in order to bond together all parts of the model. This adhesive layer is also known as bonding layer and there are multiple choices in the market respecting material, thickness, dimension, dielectric constant, etc.

During this thesis project, a bonding layer from Rogers Corporation was tested. The bonding layer is RO4450F, it has a dielectric constant of 3.52 and a standard thickness of 0.101 mm (Corporation, 2021). A layer of RO4450F material was then added to the simulation model between the upper and lower layer, and between the lower layer and the antenna interface, as shown in Figure 49. The thickness of the bonding layer is 0.101 mm and the thickness of the pads is 0.035 mm. Considering those values, the distance between pads is 0.031 mm.

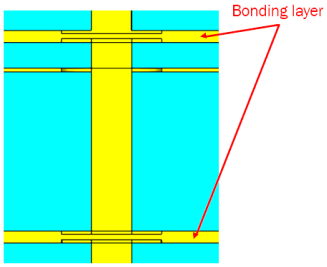

Figure 49. Close up of the model with bonding layers.

3.5.1 S-parameters

The following figures illustrate the simulation results of the 4x4 integration network model with bonding layers. There was no optimization of the rest of the parameters. Figure 50 shows the transmission and reflection coefficients of the new model.

The transmission coefficients are above -1.8 dB over 17-22 GHz, the reflection coefficients are below -8.5 dB. These results are not as good as the results of the model with air gaps, it can be due to the addition of the bonding layers and also because the rest of the parameters were not optimized until finding the best performance possible considering the new adhesive layers.

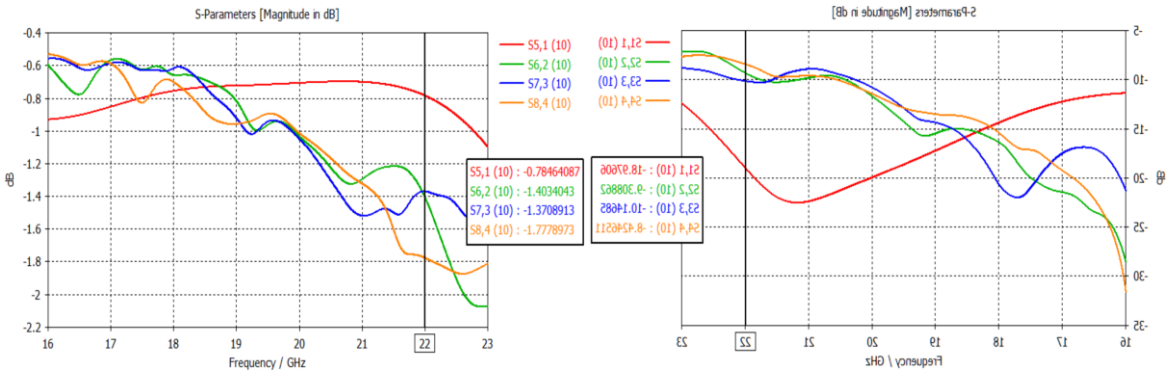

Figure 50. Transmission coefficient (left) and reflection coefficient (right) of the 4x4 array integration with bonding layers.

Mutual coupling among all ports is below -30 dB, as illustrated in Figure 51. Figure 51 also shows the same plots but in linear scale.

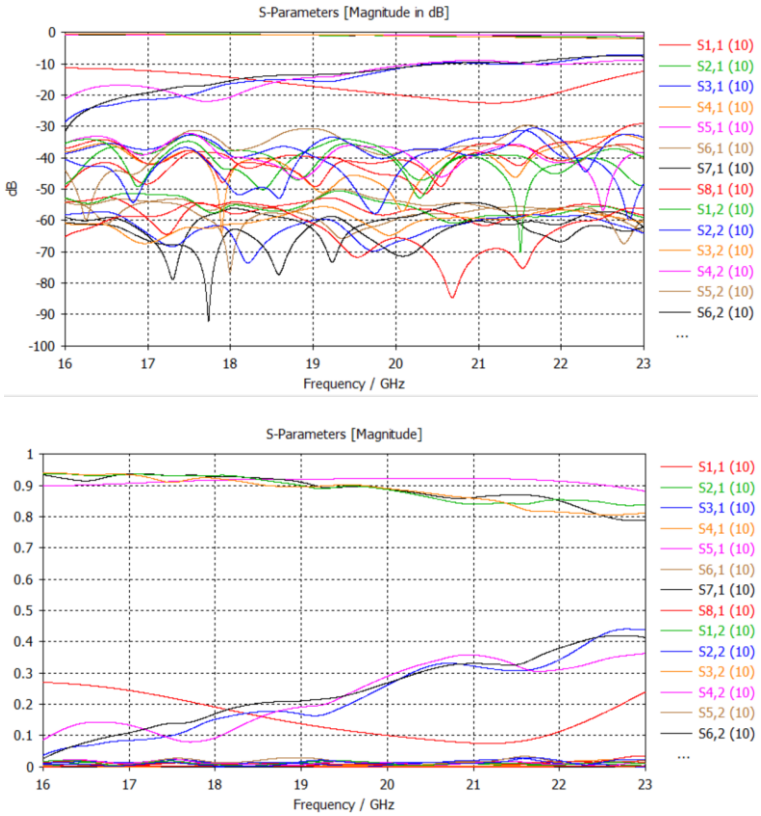

Figure 51. Figure 36. S-parameters of the model with bonding layers in dB (up) and in linear scale (down).

3.5.2 Misalignment tests

The 4x4 model with bonding layers was also simulated under misalignment conditions. In this case the model was tested along x, y and z axis. In x and y directions, the misalignment values that were used for the tests are 0.1 mm and 0.2 mm. The tests were conducted just as explained in section 3.4.3.

Respecting misalignment along z axis, the tests were done by changing the distance between pads. The selected values for the tests were 0 mm, 0.031 mm and 0.132 mm. Such values correspond to a bonding layer with thickness of 0.07 mm (a non-standard thickness dimension), 0.101 mm and 0.202 mm, respectively. In this case, 0.202 mm is not a standard thickness for this particular bonding layer, but it could be achieved by applying two bonding layers of 0.101 mm to the model.

Figure 52 shows the transmission coefficient from port 1 to port 5. A misalignment value of 0.2 mm in x and no misalignment in y, is the same of having no misalignment in x and a misalignment of 0.2 mm in y at lower frequencies.

Also, the transmission coefficient values from port 1 to port 5 under no misalignment conditions are above -0.8 dB over 17-22 GHz, it dropped to -0.9 dB with misalignment conditions along x or y axis and it dropped again to -1 dB under misalignment conditions along x and y axes combined. So, having a misalignment in both directions at the same time, is roughly twice the effect on the model of a misalignment in only one direction at lower frequencies.

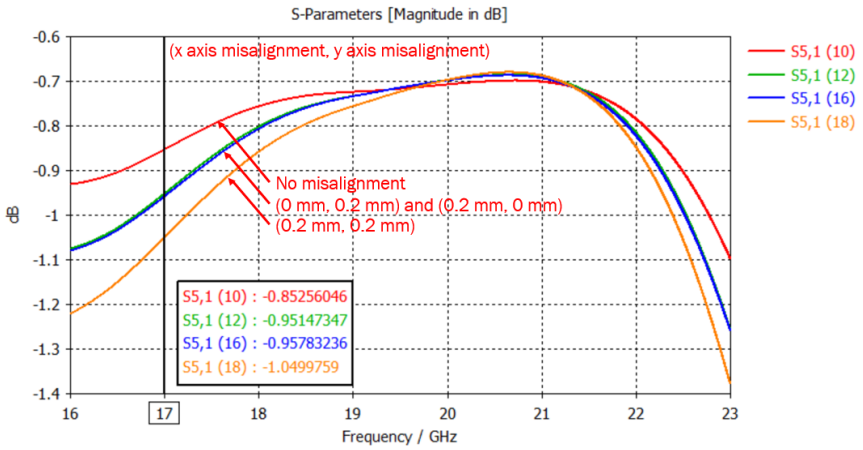

Figure 52. Transmission coefficient from port 1 to 5 with bonding layers under x and y misalignment conditions.

The reflection coefficient of port 1 has similar effects under misalignment conditions. Figure 53 shows the corresponding plots.

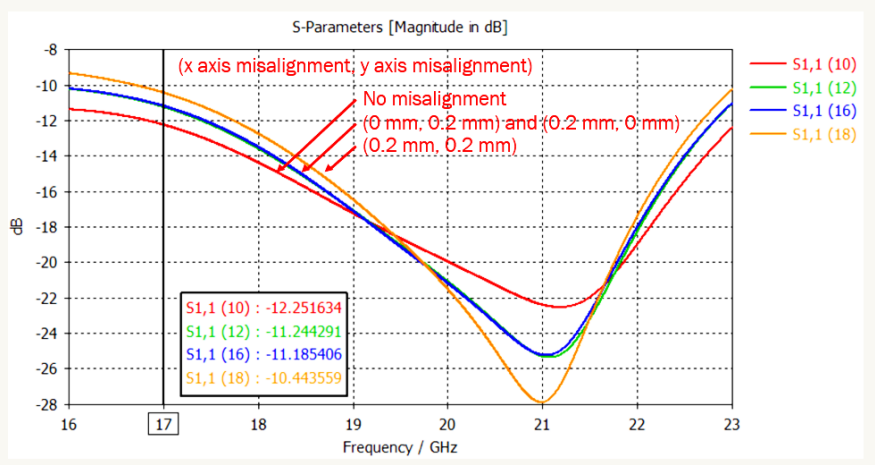

Figure 53. Reflection coefficient of port 1 with bonding layers under x and y misalignment conditions.

Figure 54 show the corresponding comparison of the transmission coefficients from port 1 to 5 when applying misalignment values along x and y axes from 0.1 mm to 0.2 mm. And Figure 55 shows the reflection coefficient of port 1 under the same conditions.

Port 1 performance was also the most affected during the misalignment tests. It has transmission coefficient values above -0.8 dB over 17-22 GHz with no misalignments and transmission coefficient values above -1 dB over the same frequency range under the maximum tested misalignment conditions along x and y axis. On the other hand, the reflection coefficient went from values below -12.2 dB to -10.4 dB.

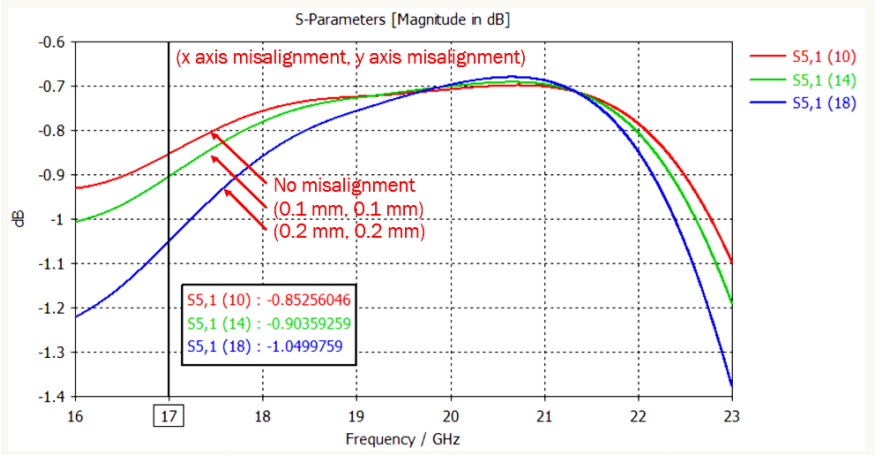

Figure 54. Transmission coefficient from port 5 to port 1 with bonding layers under maximum tested x and y misalignment conditions.

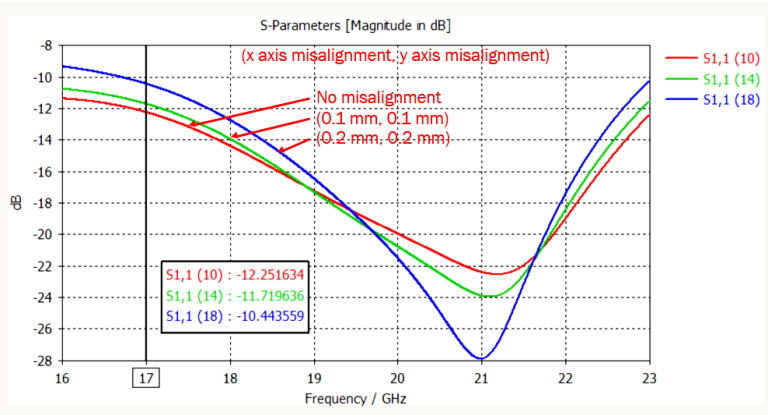

Figure 55. Reflection coefficient of port 1 with bonding layers under maximum tested x and y misalignment conditions.

For misalignment tests along z axis, the gap between copper pads was changed to study its effects on the model performance. Increasing the gap had an effect on the model's bandwidth as shown in Figures 56 and 57. The operation bandwidth of the model moves to higher frequencies as the size of the gap increases. Also, the coupling increases with smaller gaps.

Plots of the model performance of ports 1 to 4 under variations of the gap in dB and linear scale can be found in the Annex.

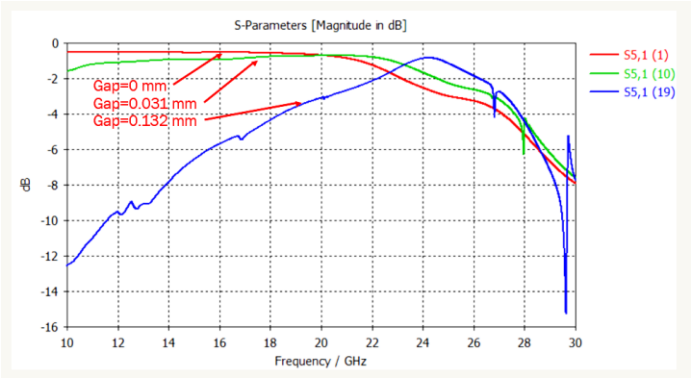

Figure 56. Transmission coefficient of the model with bonding layers, port 1 to 5 with different gap values.

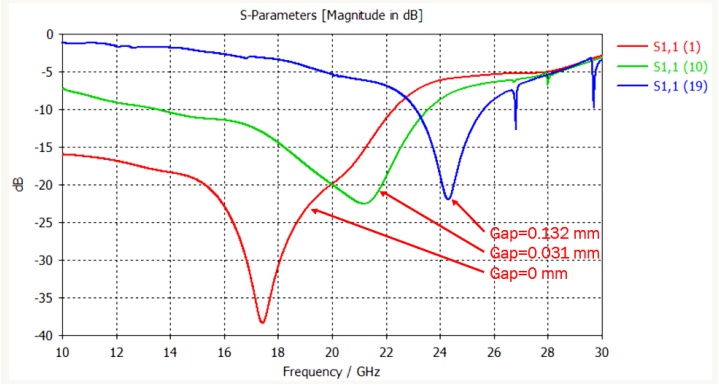

Figure 57. Reflection coefficient of the model with bonding layers, port 1 with different gap values.

4

4. Discussion

Preliminary tests on the fully contactless MetaCoax technology without optimization, present reflection coefficient values below -8 dB, mutual coupling below -50 dB and transmission coefficient values above -1.5 dB, over 22-42 GHz.

In this thesis, the 2x2 integration network model designed with MetaCoax technology, shows reflection coefficient values below -10 dB, mutual coupling below -50 dB and transmission coefficient values above -1 dB, over 17-22 GHz.

On the other hand, the 4x4 integration network model, also designed with MetaCoax technology, shows reflection coefficient values below -10 dB, mutual coupling below -30 dB and transmission coefficient values above -1.4 dB, over 17-22 GHz.

The results obtained from the 2x2 and 4x4 integration network models are consistent with the results of the preliminary tests on the fully contactless MetaCoax technology without optimization. The 2x2 integration network model has slightly better mutual coupling and transmission coefficient values than the 4x4 model over 17-22 GHz.

The 2x2 model design considers only one air gap between the integration network and the antenna interface, while the 4x4 model has two air gaps, one air gap between the integration network upper and lower layers and one air gap between the integration network lower layer and the antenna interface. So, the signal has to go through up to two air gaps for some of the ports in the 4x4 model, while the signal in all ports of the 2x2 model has to go through only one air gap. Also, the 4x4 model has longer microstrip lines than the 2x2 model. Such facts may explain the slightly higher transmission coefficient values observed in the 2x2 model.

Both simulation models were optimized and most of their parameters were tunned until having an acceptable performance over 17-22 GHz. Nevertheless, the 4x4 integration network model optimization was more challenging due to the nature of its design, since some ports have different layer configuration and thus different performance.

In the particular cases presented in this thesis, port 2, 3 and 4 of the 4x4 model have similar results, and they differ from port 1 results, but the optimization

procedure was applied until having the best performance possible over 17-22 GHz for all ports.

Misalignment tests along x and y axes separately were found to have the same effect on the 4x4 model performance. For example, considering a misalignment value of 0.1 mm in x and no misalignment in y, is the same of having no misalignment in x and a misalignment of 0.1 mm in y. This can be explained by the circular geometry of the pads, since moving some layers of the model along x axis will result the same as moving the layers along y axis.

The results also showed linear effects on the model performance during misalignment tests along x and y axes over the lower frequencies of the range. For example, the transmission coefficient values from port 1 to port 5 under no misalignment conditions are above -1.1 dB, it dropped to -1.2 dB with misalignment conditions along x or y axis and it dropped again to -1.3 dB under misalignment conditions along x and y axes combined. So, having a misalignment in both directions at the same time, is like having roughly twice the effect on the model of a misalignment in only one direction.

Port 1 performance was the most affected during the misalignment tests. It has transmission coefficient values above -1.1 dB over 17-22 GHz with no misalignment and transmission coefficient values above -2 dB over the same frequency range under the maximum tested misalignment conditions along x and y axis. On the other hand, the reflection coefficient went from values below -10 dB to -6.6 dB.

Mutual coupling remained the same, below -30 dB over 17-22 GHz, even under misalignment conditions.

During misalignment tests along z axis, the air gap between copper pads was changed in order to study its effects on the model performance. Increasing the gap had an effect on the model's bandwidth.

Apparently, the operation bandwidth of the model moves to higher frequencies as the size of the gap increases. Also, it seems that the coupling increases with smaller gaps. These results suggest that the effects are due to the capacitive coupling of the MetaCoax technology.

Regarding the simulation of the 4x4 integration network with bonding layers in the design, the results suggest that the model is less sensitive to changes in the dimension of the gap between pads at higher dielectric constant values of the bonding layer material. Also, the model is less sensitive to misalignment along x and y axes at higher dielectric constant values of the bonding layer.

Misalignment tests on the 4x4 model with bonding layers had similar results to the model with air gaps. After analyzing the results of the tests, misalignments along x and y axes separately, have the same effects on the S-parameters. Similarly, the

model kept the linear effects on its performance during misalignment tests along x and y axes, since the effect of having a misalignment in both directions at the same time, is roughly twice the effect on the model of a misalignment in only one direction.

The tests of the 4x4 integration model with bonding layers also show capacitive coupling effects, since the operation bandwidth of the model moves to higher frequencies as the size of the gap between pads increases and the coupling increases with smaller gap values.

This master thesis project is a first study of MetaCoax as a solution for integration technologies over 17 GHz to 22 GHz and it can be seen as a cost-effective solution compared to existing technology like tiling or RF-optic transformers. The next step is adjusting the model in order to manufacture a physical prototype and perform measurements. In that way, simulations and measurements can be compared and studied.

The integration solution presented in this thesis is aimed to work with a 4x4 circularly-polarized antenna array. So, another important next step is to replace the antenna interface used in this thesis during simulations with the actual antenna array model. Then, study the outcomes and compare the performance of the antenna array alone and the antenna array with the integration network to conclude on the effects that the integration solution has over the antenna array.

More simulation work is needed in order to know more about the phase of the transmitted signals from the different ports and adjust the model if necessary. Since the integration network is designed to work with an antenna array, the phase is then an important element to take into account. Preliminary simulation tests show that the transmitted signals from ports 2, 3 and 4 have the same phase, but port 1 is different.

The gaps between layers could reduce heat dissipation issues of multilayer PCBs, but more tests are required to measure the actual improvement of this solution.

Other interesting studies include extending the range of the gaps between conductive elements and the range of frequencies, since according to the results of this thesis, it is probable that the integration network design with MetaCoax can have also a good performance at frequencies above 25 GHz by just making some adjustments to the model.

Some more tests with different bonding layer materials can be performed in order to conclude on the best material and dimensions of a bonding layer for a prototype over a specific frequency range.

Finally, another possible future work for this thesis is extending the current 4x4 integration network to a bigger model, for example a 6x6 or 8x8 model, in order to study the outcomes of more complex designs based on MetaCoax.

5

5. Conclusions

This thesis presents a 4x4 integration network solution based on fully contactless MetaCoax technology, it was designed and simulated using CST. The integration solution is optimized to work over 17-22 GHz and it is designed to work with an antenna array with a separation of 7 mm between elements.

Results from simulations show reflection coefficient values below -10 dB, mutual coupling below -30 dB and transmission coefficient values above -1.4 dB. This implies that the solution has low losses and the electromagnetic band-gap structure designed to stop leakage and mutual coupling works.

Simulation results suggest capacitive coupling effects are present on the model. The operation bandwidth of the model moves to higher frequencies as the size of the gap between layers increases and the coupling increases with smaller gaps.

Misalignment tests were performed on the model. The results show that the model is robust against alignment errors along x and y axes.

Also, it was found that misalignment has linear effects on the S-parameters, since having a misalignment along x and y axes at the same time, is like having roughly twice the effect on the model of a misalignment in only one direction.

The integration solution using MetaCoax is very flexible regarding size and configuration. Nevertheless, the optimization procedure can be challenging for bigger integration networks.

The air gaps between layers of the integration network could reduce heat dissipation issues of multilayer PCBs, but more tests are required to measure the actual improvement of this solution.

Also, it was presented an option for manufacturing a prototype by using bonding layers to bond together the different parts of the model.

The bonding layers are used instead of the original air gaps. The model with this variation has a similar performance and it is also robust against alignment errors. Yet, more studies are required in order to analyze the effects of the dielectric constant and thickness of different bonding layer materials and select the most appropriate for a specific frequency range.

It was demonstrated that the cost effective fully contactless MetaCoax technology can be used as an integration solution and it can be used to address the space limitation problem due to the small separation between antenna array elements at mmWave bands.

6

6. Annex

6.1 Transmission and reflection coefficients of 4x4 array integration

6.1.1 Port 1

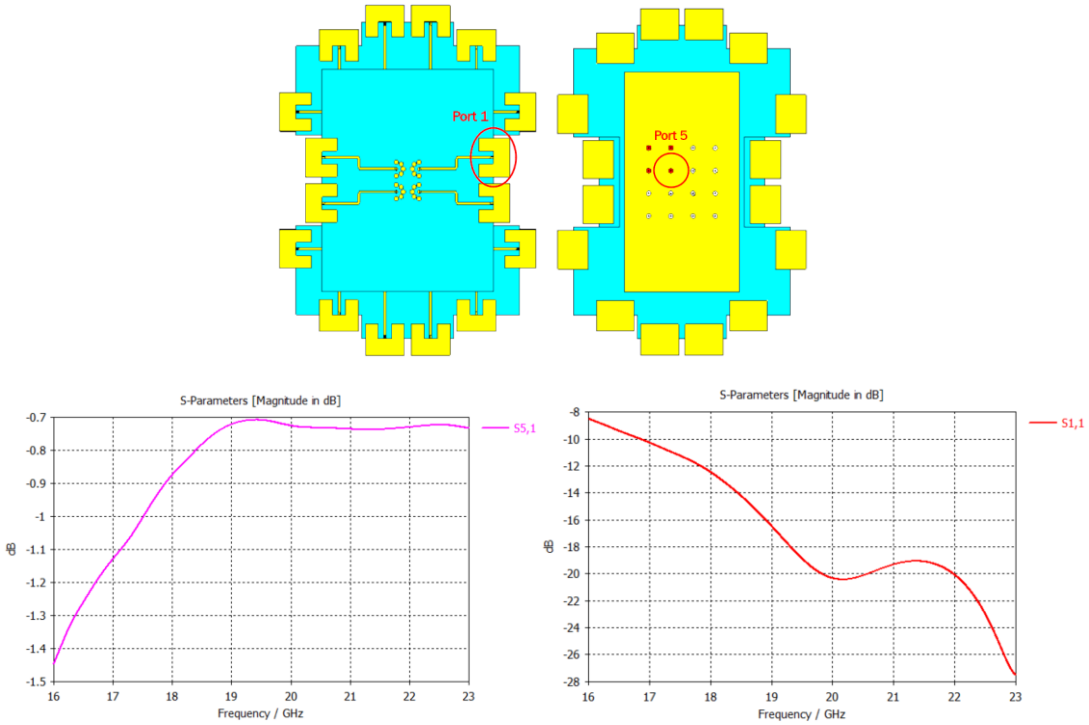

Transmission coefficient port 1 to 5 (left) and reflection coefficient port 1 (right).

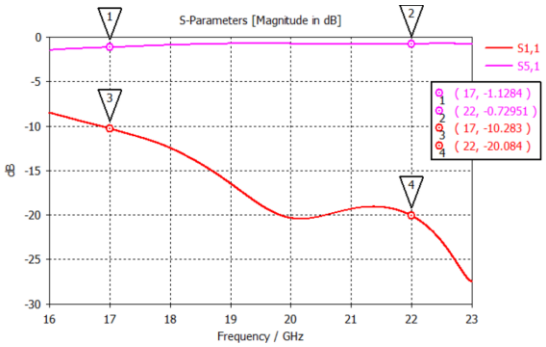

S(5,1) and S(1,1)

6.1.2 Port 2

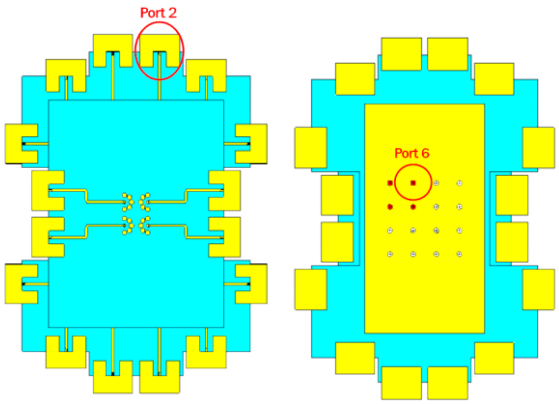

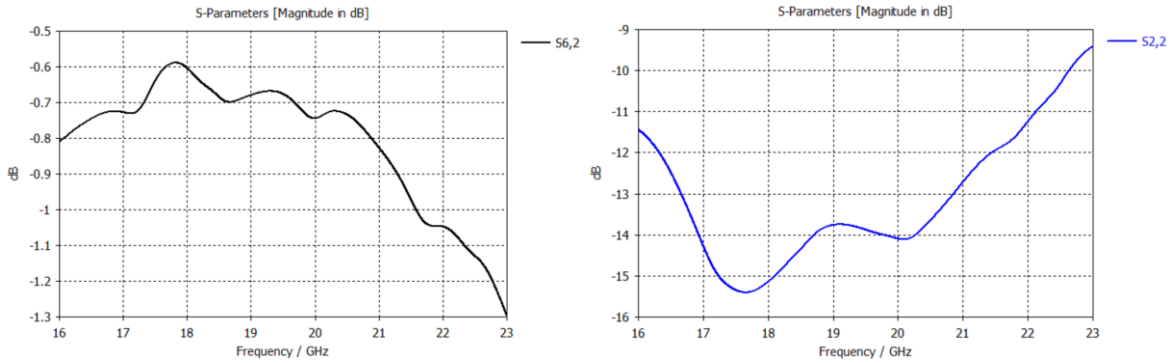

Transmission coefficient port 2 to 6 (left) and reflection coefficient port 2 (right).

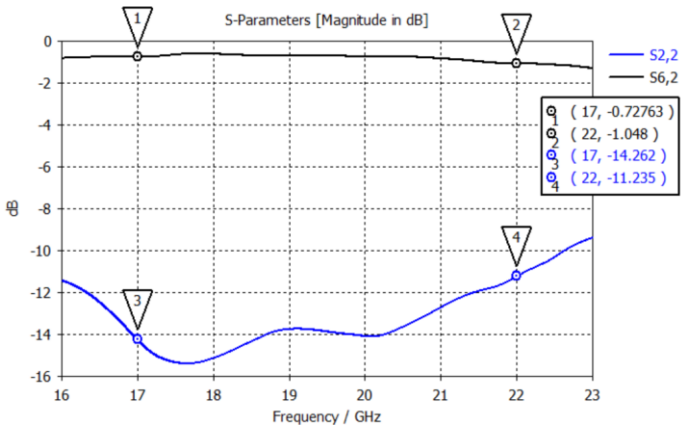

S(6,2) and S(2,2)

6.1.3 Port 3

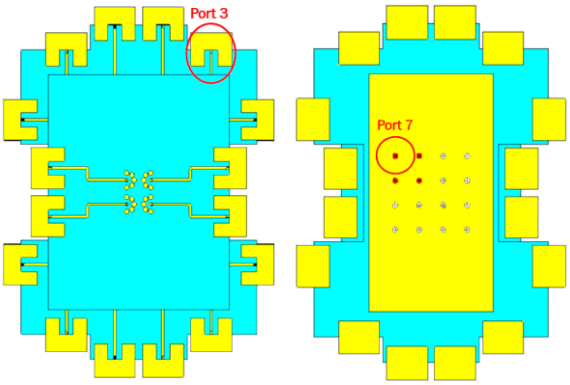

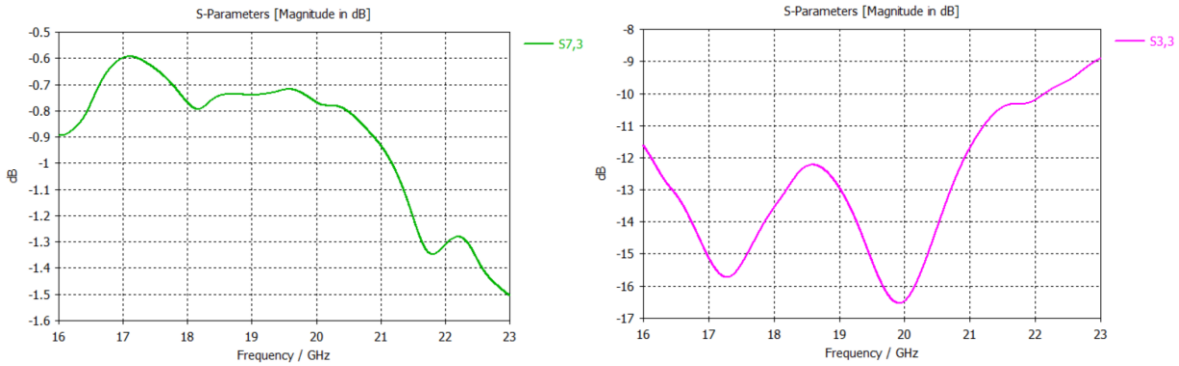

Transmission coefficient port 3 to 7 (left) and reflection coefficient port 3 (right).

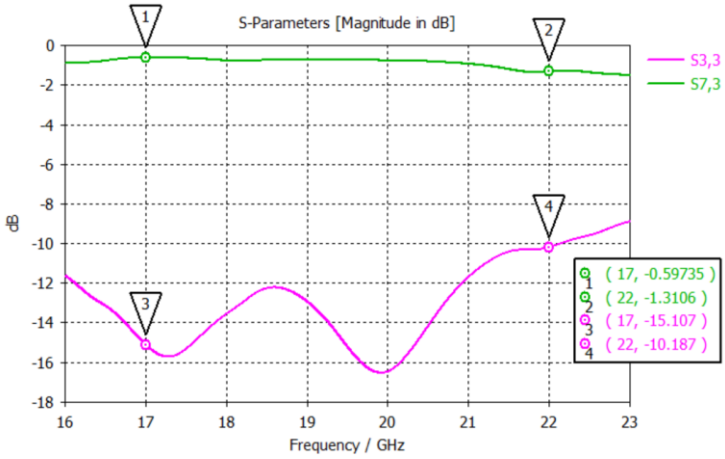

S(7,3) and S(3,3)

6.1.3 Port 4

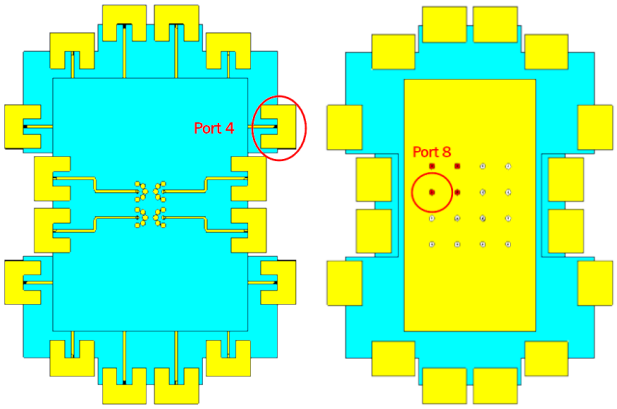

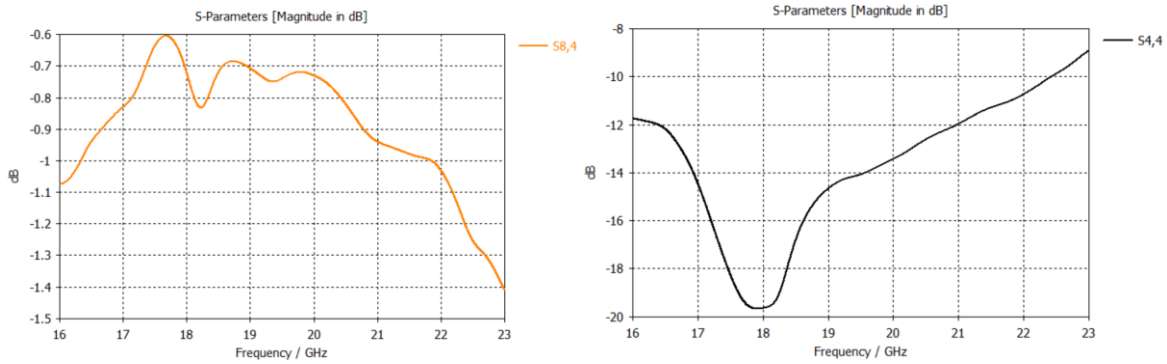

Transmission coefficient port 4 to 8 (left) and reflection coefficient port 4 (right).

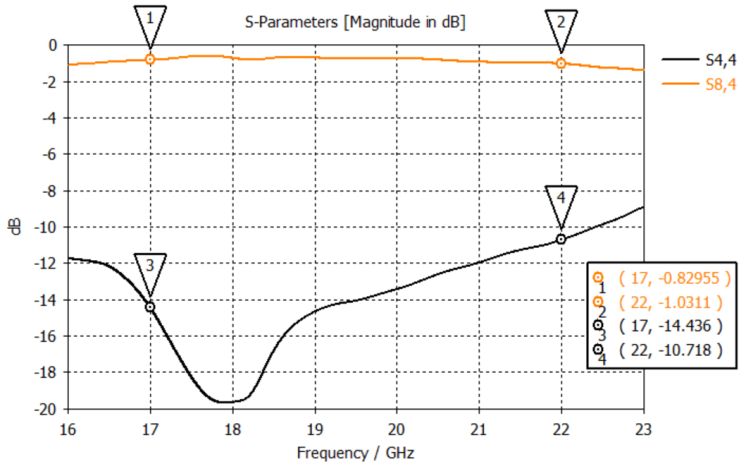

S(8,4) and S(4,4)

6.2 Transmission and reflection coefficients of 4x4 feeding network with air gap variations

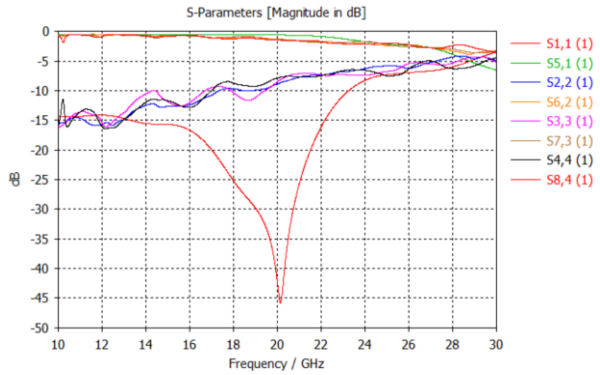

Transmission and reflection coefficients with airgap = 0 mm [in dB].

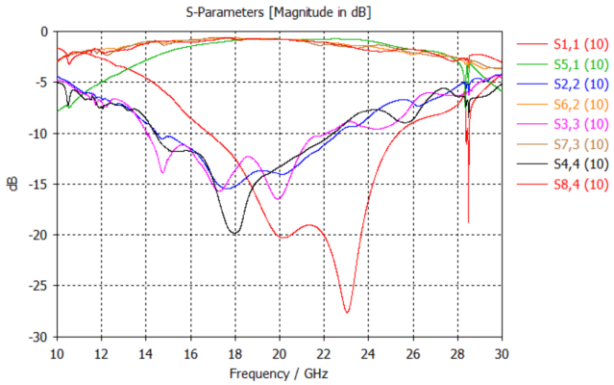

Transmission and reflection coefficients with airgap = 0.05 mm [in dB].

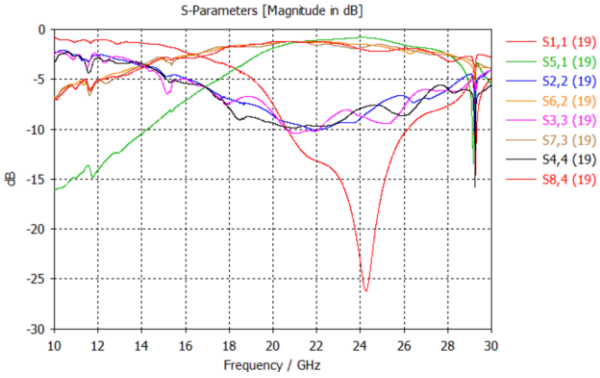

Transmission and reflection coefficients with airgap = 0.1 mm [in dB].

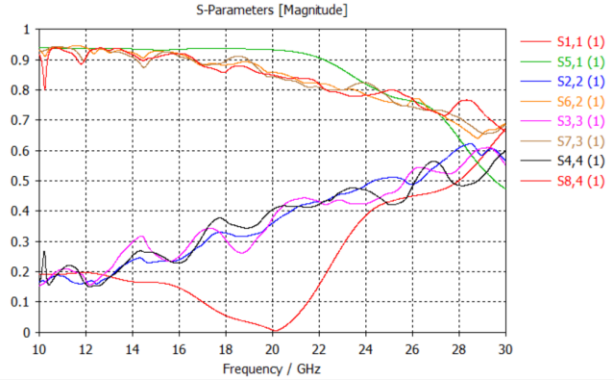

Transmission and reflection coefficients with airgap = 0 mm [in linear scale].

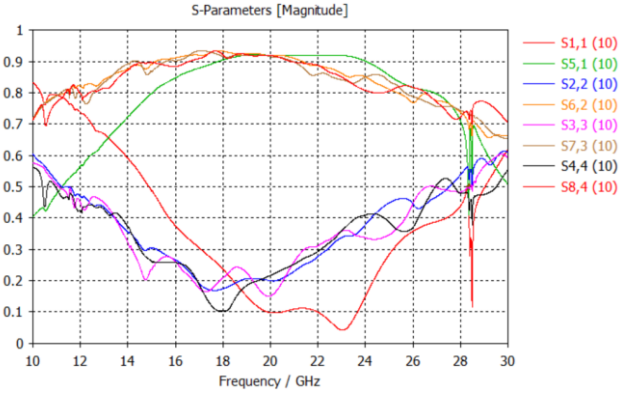

Transmission and reflection coefficients with airgap = 0.05 mm [in linear scale].

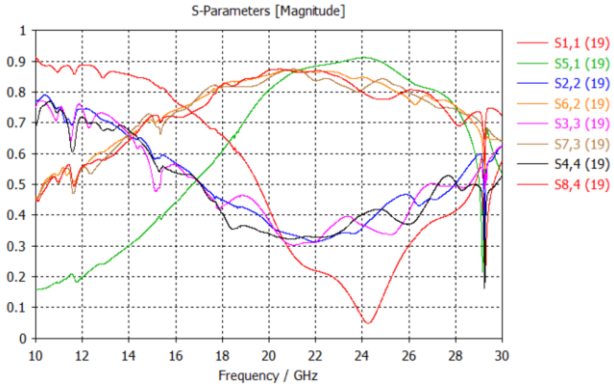

Transmission and reflection coefficients with airgap = 0.1 mm [in linear scale].

6.3 Transmission and reflection coefficients of 4x4 feeding network with bonding layers

6.3.1 Port 1

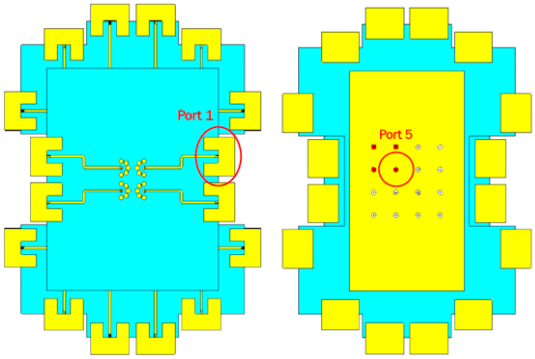

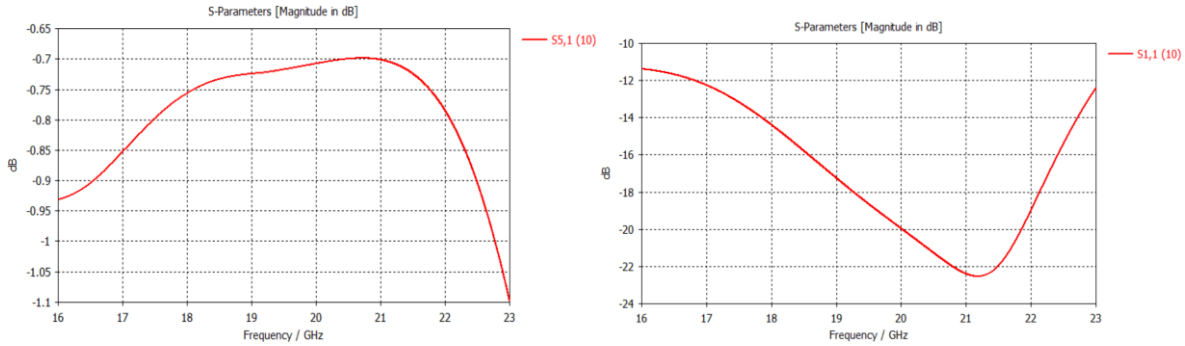

Transmission coefficient port 1 to 5 (left) and reflection coefficient port 1 (right).

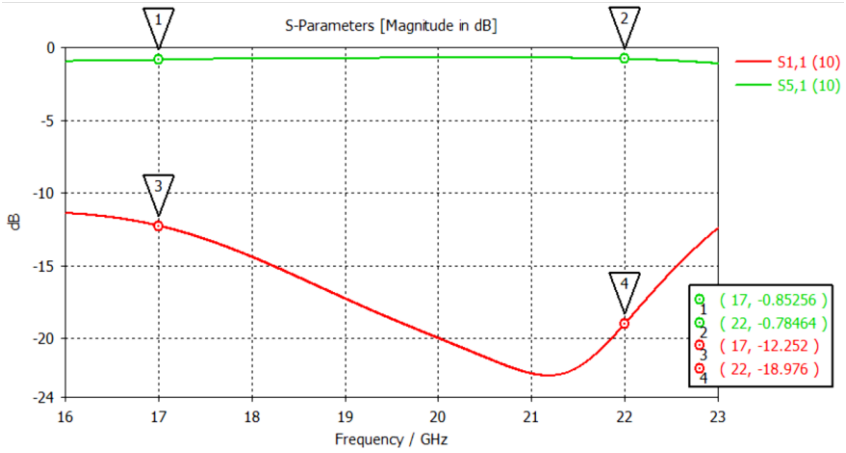

S(5,1) and S(1,1)

6.3.2 Port 2

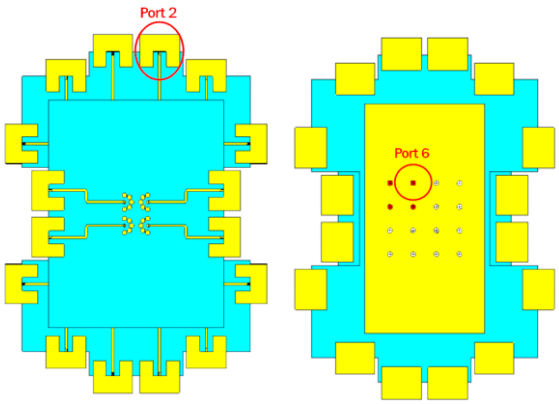

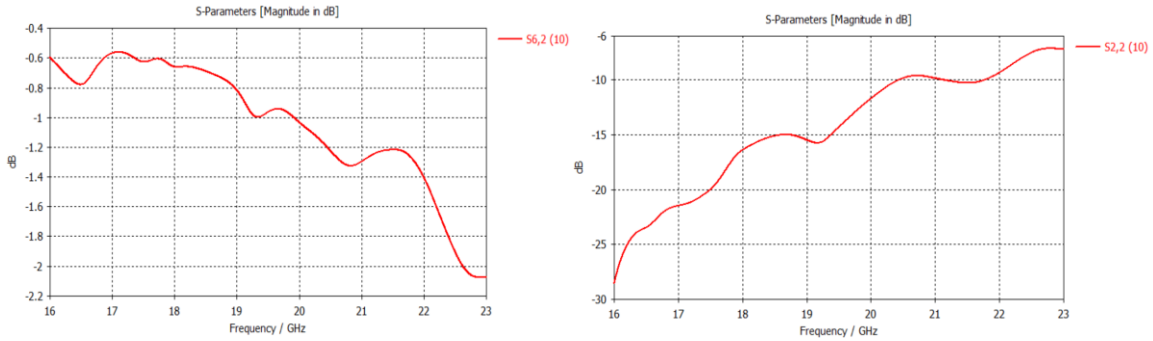

Transmission coefficient port 2 to 6 (left) and reflection coefficient port 2 (right).

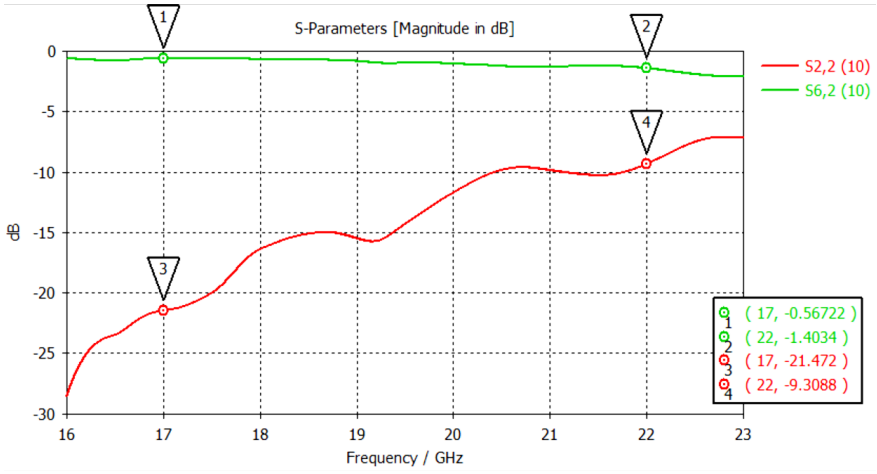

S(6,2) and S(2,2)

6.3.3 Port 3

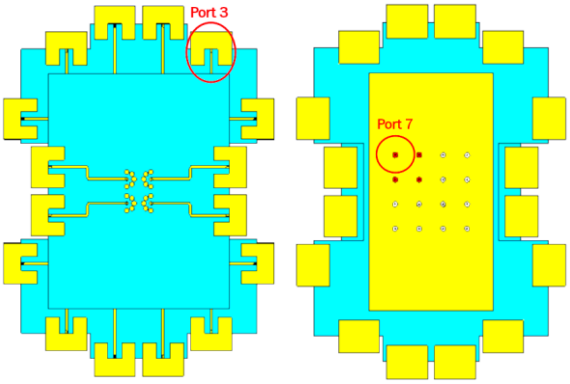

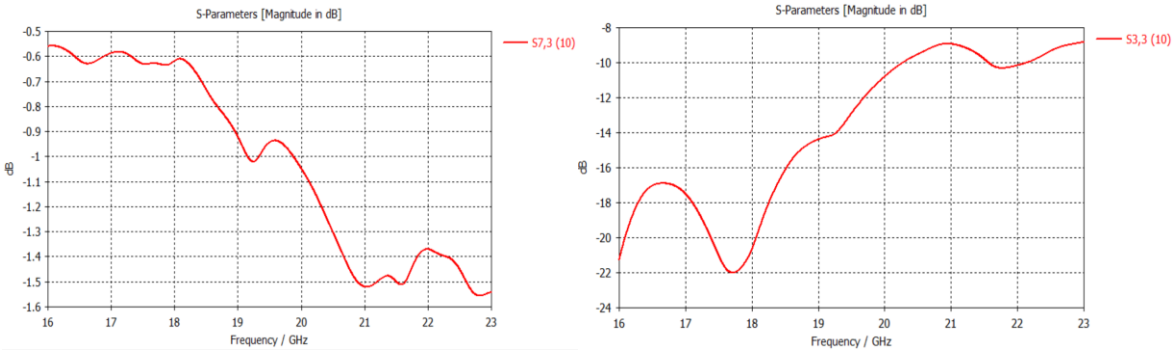

Transmission coefficient port 3 to 7 (left) and reflection coefficient port 3 (right).

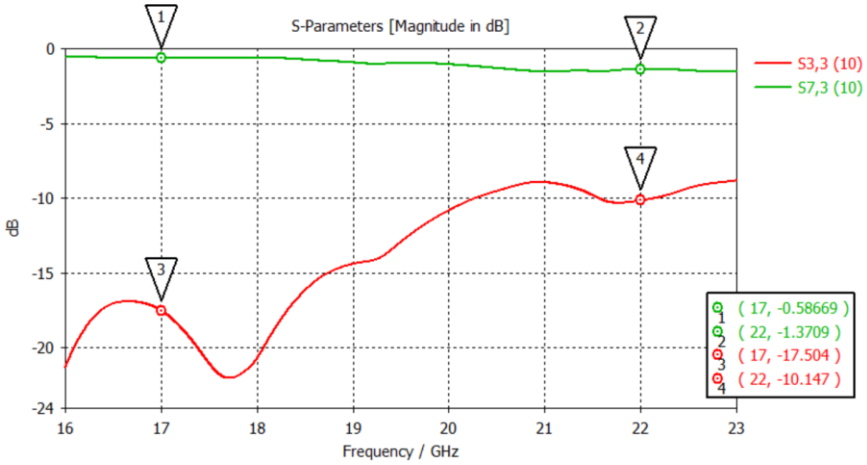

S(7,3) and S(3,3)

6.3.4 Port 4

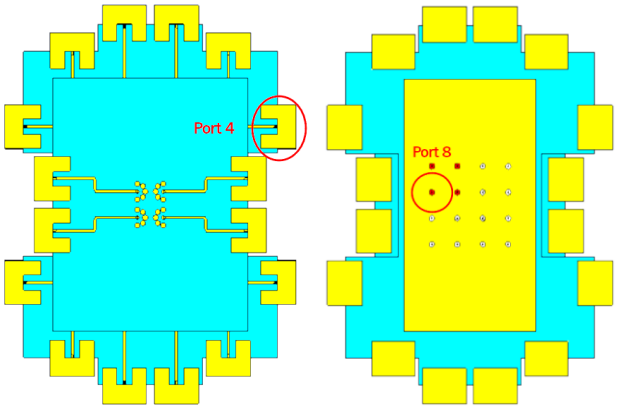

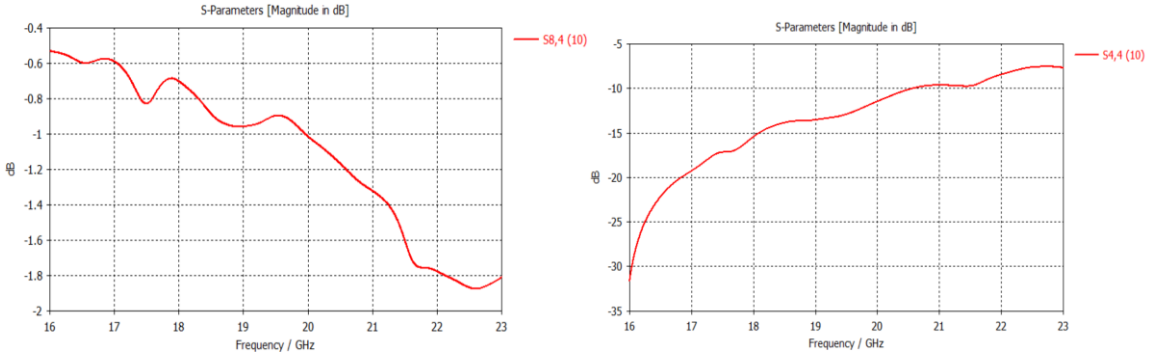

Transmission coefficient port 4 to 8 (left) and reflection coefficient port 4 (right).

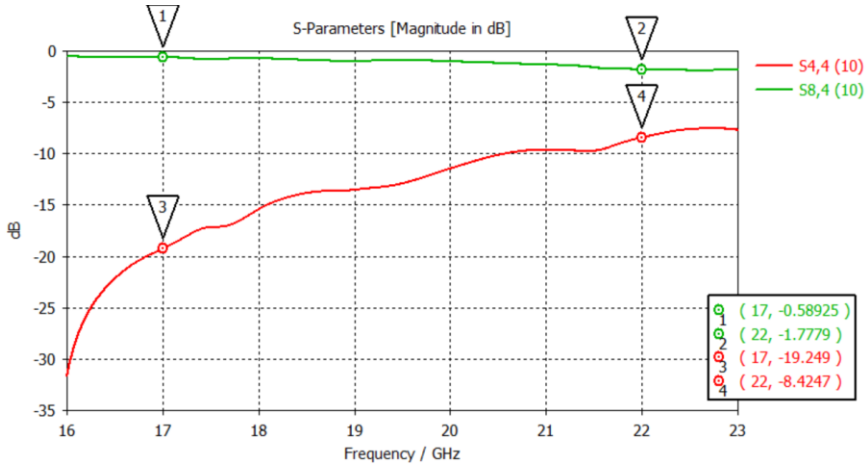

S(8,4) and S(4,4)

6.4 Transmission and reflection coefficients of 4x4 feeding network with bonding layers and gap variations

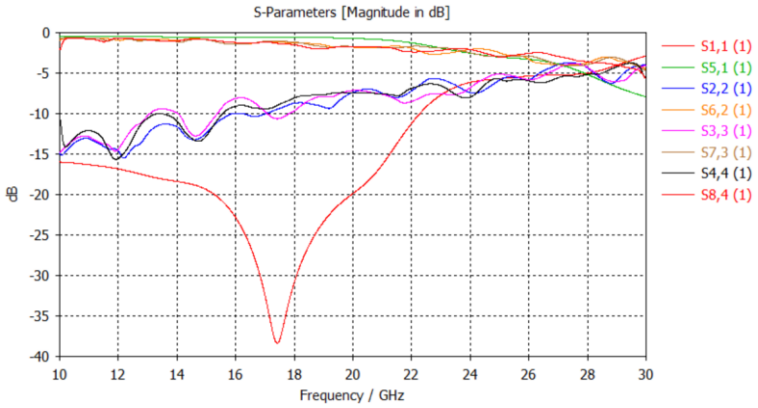

Transmission and reflection coefficients with gap = 0 mm [in dB].

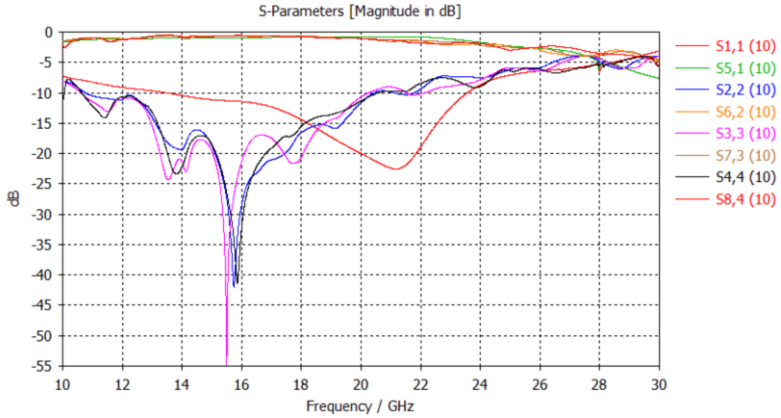

Transmission and reflection coefficients with gap = 0.031 mm [in dB].

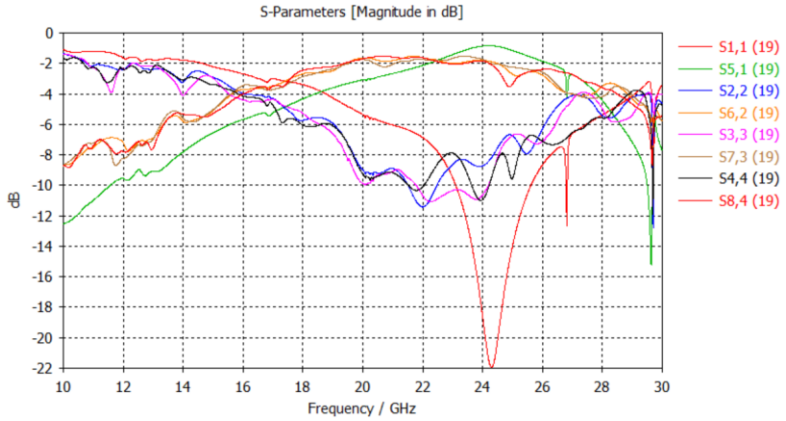

Transmission and reflection coefficients with gap = 0.132 mm [in dB].

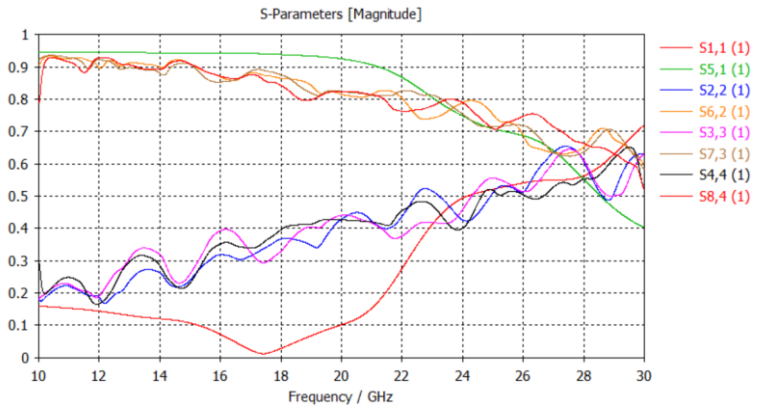

Transmission and reflection coefficients with gap = 0 mm [in linear scale].

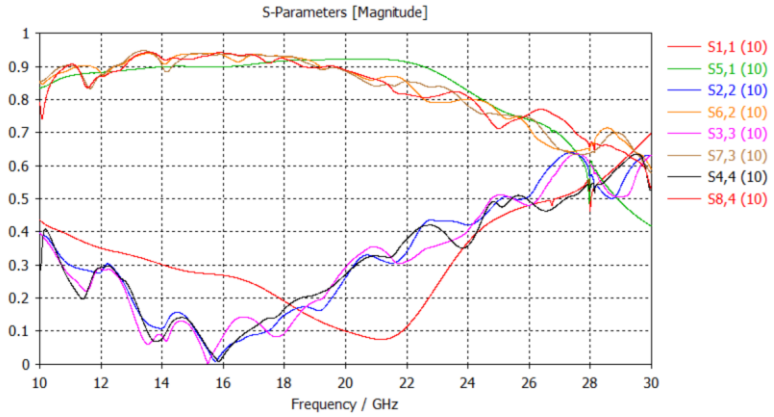

Transmission and reflection coefficients with gap = 0.031 mm [in linear scale].

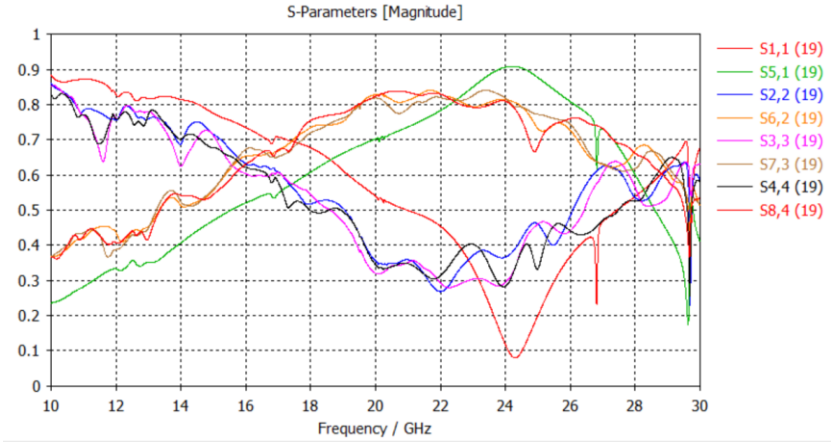

Transmission and reflection coefficients with gap = 0.1 mm [in linear scale].

7

7. References

Bhowmik, L., & Fulton, C. (2016). Analysis and Measurement of Grating Lobe Effects in Infinite Planar Arrays of Finite-Sized Subarrays. *Conference paper.*, DOI: 10.1109/ARRAY.2016.7832617.

Cryan, W., & et. al. (2004). A 2.4GHz wireless-over-fibre transmitter using a VCSEL-based photonic active integrated antenna (PhAIA). *34th European Microwave Conference*, 507-509.

Eu, G. C., & et. al. (2017). A Printed Array Antenna for Multi-layer PCB Design. *Conference Paper*.

Fukumori, T., & et. al. (2012). Characterization of Signal Via Structure in Multilayer Printed Circuit Boards up to 50 GHz. *2nd IEEE CPMT Symposium Japan* .

GSMA. (2021). *5G Spectrum Guide – Everything You Need to Know*. Retrieved from https://www.gsma.com/spectrum/5g-spectrum-guide/

Jaehyun Choi, e. a. (2020). Frequency-Adjustable Planar Folded Slot Antenna Using Fully Integrated Multithrow Function for 5G Mobile Devices at Millimeter-Wave Spectrum. *IEEE Transactions on Microwave Theory and Techniques*.

Nazhan, S., & et. al. (2021). Experimental Demonstration of an Ultra-Low Power Vertical-Cavity Surface-Emitting Laser for Optical Power Generation. *International Journal of Electronics and Communication Engineering*.

Rahayu, Y., Rahman, T. A., Ngah, R., & Hall, P. (2008). Ultra Wideband Techonology and Its Applications. *IEEE*.

Safaisini, R., & et. al. (2012). High-Speed 850 nm Quasi-Single Mode VCSELs for Extended Reach Optical Interconnects. *Journal of Optical Communications and Networking*.

Westbergh, P., & et. al. (2012). High-speed 850 nm VCSELs with 28 GHz modulation bandwidth operating error-free up to 44 Gbit/s. *Electronic Letters*.

Zhang, T., & et. al. (2020). Ultra-wideband Linearly Polarized Planar Bowtie Array Antenna with Feeding Network using Dielectric-based Inverted Microstrip Gap Waveguide. *IET Microwaves, Antennas & Propagation*.

Zhongxia, a., & et. al. (2017). Optoelectronics Enabled Dense Patch Antenna Array for Future 5G Cellular Applications. *IEEE.*, DOI: 10.1109/ecoc.2017.8346107 .

DEPARTMENT OF ELECTRICAL ENGINEERING,
ANTENNA RESEARCH GROUP
CHALMERS UNIVERSITY OF TECHNOLOGY
Gothenburg, Sweden 2021
www.chalmers.se

CHALMERS
UNIVERSITY OF TECHNOLOGY